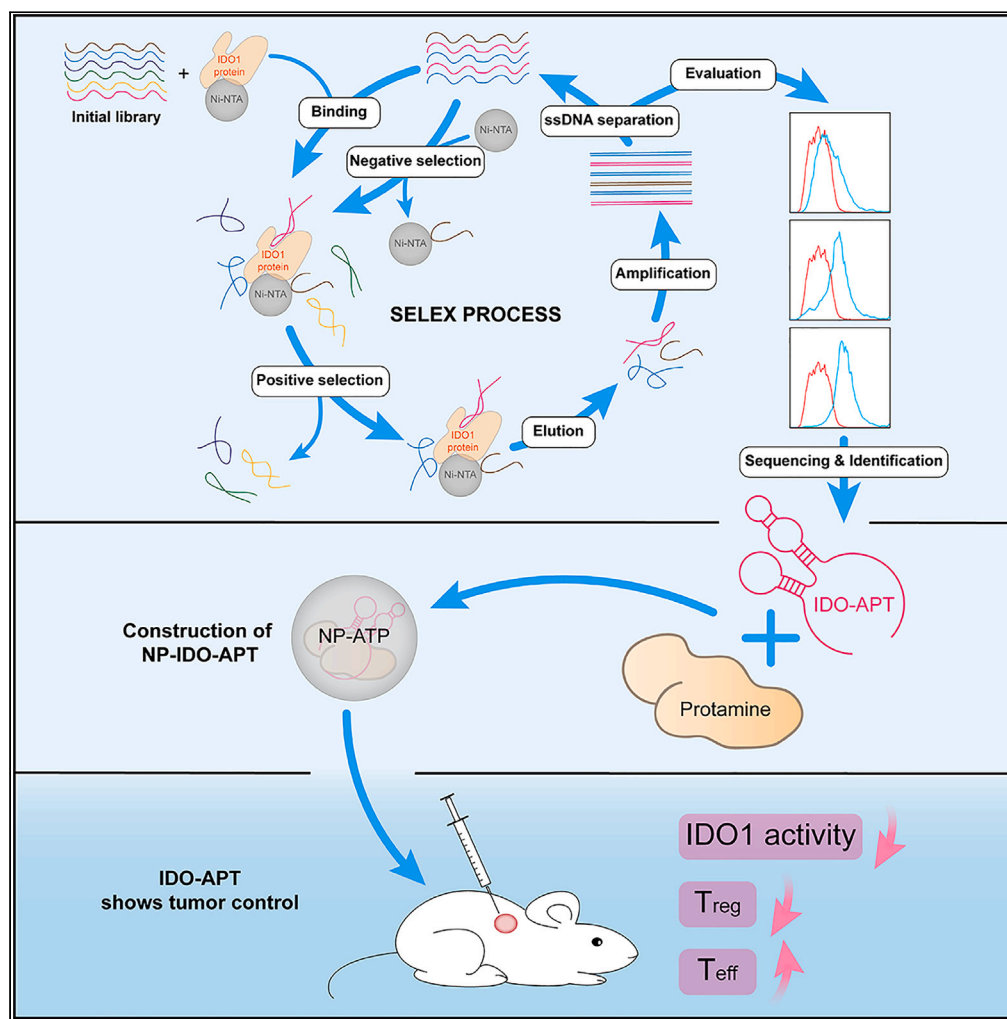**Article**

Development of a DNA aptamer targeting IDO1 with anti-tumor effects

Zhenyu Zhu,
Zeliang Yang,
Chuanda Zhu, ...,
Xi Chen, Yan Jin,
Yuxin Yin

yinyuxin@bjmu.edu.cn

Highlights

IDO-APT specifically binds IDO1 and inhibits its enzyme activity

IDO-APT internalized into cells by conjugating with nanoparticles

IDO-APT suppresses tumor growth and enhances immune response

Article

Development of a DNA aptamer targeting IDO1 with anti-tumor effects

Zhenyu Zhu,[1] Zeliang Yang,[1] Chuanda Zhu,[1] Zixi Hu,[1] Zhongyu Jiang,[1] Jingjing Gong,[1] Yuyao Yuan,[1] Xi Chen,[1] Yan Jin,[1] and Yuxin Yin[1,2,3,4,*]

SUMMARY

Immune checkpoint blockade has become an effective approach to reverse the immune tolerance of tumor cells. Indoleamine 2,3-dioxygenase 1 (IDO1) is frequently upregulated in many types of cancers and contributes to the establishment of an immunosuppressive cancer microenvironment, which has been thought to be a potential target for cancer therapy. However, the development of IDO1 inhibitors for clinical application is still limited. Here, we isolated a DNA aptamer with a strong affinity and inhibitory activity against IDO1, designated as IDO-APT. By conjugating with nanoparticles, _in situ_ injection of IDO-APT to CT26 tumor-bearing mice significantly suppresses the activity of regulatory T cells and promotes the function of CD8$^+$ T cells, leading to tumor suppression and prolonged survival. Therefore, this functional IDO1-specific aptamer with potent anti-tumor effects may serve as a potential therapeutic strategy in cancer immunotherapy. Our data provide an alternative way to target IDO1 in addition to small molecule inhibitors.

INTRODUCTION

Cancers build up an immunosuppressive tumor microenvironment by upregulating the expression of immune checkpoints to achieve immune escape.[1] Thus, immune checkpoints have become promising targets in cancer therapy. In recent years, immune checkpoint inhibitors (ICIs) have been widely applied and have improved clinical outcomes in a variety of malignancies.[2] Indoleamine 2,3-dioxygenase 1 (IDO1), a heme-containing dioxygenase, as a classical immune checkpoint is thought to contribute to tumor immune escape.[3] IDO1 involves the rate-limiting step of tryptophan (Trp) metabolism, converting Trp to kynurenine (Kyn).[4] High levels of IDO1 in cancers have been shown to be associated with a poor prognosis.[5] In the tumor microenvironment, overexpressed IDO1 plays an immunosuppressive role by depriving Trp, meanwhile producing Kyn and downstream catabolites—the endogenous ligand of the aryl hydrocarbon receptor (AhR), which promotes the differentiation of regulatory T (T$_{reg}$) cells and impairs the function of effector T cells.[6–8] IDO1 is a highly promising target of cancer immunotherapy, and numerous chemical inhibitors of IDO1, including indoximod (1-methyl-D-tryptophan, 1-MT) and epacadostat (INCB024360), have been developed.[9–11] However, although some of these reported inhibitors have entered clinical trials and showed effects in overcoming immune suppression, the clinical development of IDO1 inhibitors was unprosperous. Therefore, in addition to IDO1-targeting small molecule drug discovery, designing new IDO1-targeting agents may be a feasible approach.

Aptamers, first isolated in 1990, are single-stranded DNA or RNA oligonucleotides.[12,13] Due to their ability to form complex three-dimensional (3D) structures, aptamers can bind to different targets in an antibody-like manner with high specificity and affinity.[14] Compared to traditional antibodies, aptamers are more stable, less immunogenic, and easier to synthesize and modify.[15] Taking advantage of the systematic evolution of ligands by exponential enrichment (systematic evolution of ligands by exponential enrichment [SELEX]), aptamers can be isolated efficiently.[16] Over the past few decades, aptamers have been exploited in various fields, and numerous therapeutics have been developed from them.[17] Aptamer-based therapeutics generally function as carriers, antagonists, or agonists.[18–21] To date, a series of aptamers that target immune checkpoints, such as PD-1, PD-L1, CTLA-4, and LAG-3, have been reported.[21–25]

Given the sophisticated selection of aptamers, our aim is to isolate a functional aptamer antagonist with IDO1. We employed protein-based SELEX to screen for IDO1-targeted aptamers. To identify an aptamer

[1]Institute of Systems Biomedicine, Department of Pathology, Beijing Key Laboratory of Tumor Systems Biology, School of Basic Medical Sciences, Peking University Health Science Center, Beijing 100191, China

[2]Peking-Tsinghua Center for Life Sciences, Peking University Health Science Center, Beijing, China

[3]Institute of Precision Medicine, Peking University Shenzhen Hospital, Shenzhen 518036, China

[4]Lead contact

*Correspondence: yinyuxin@bjmu.edu.cn

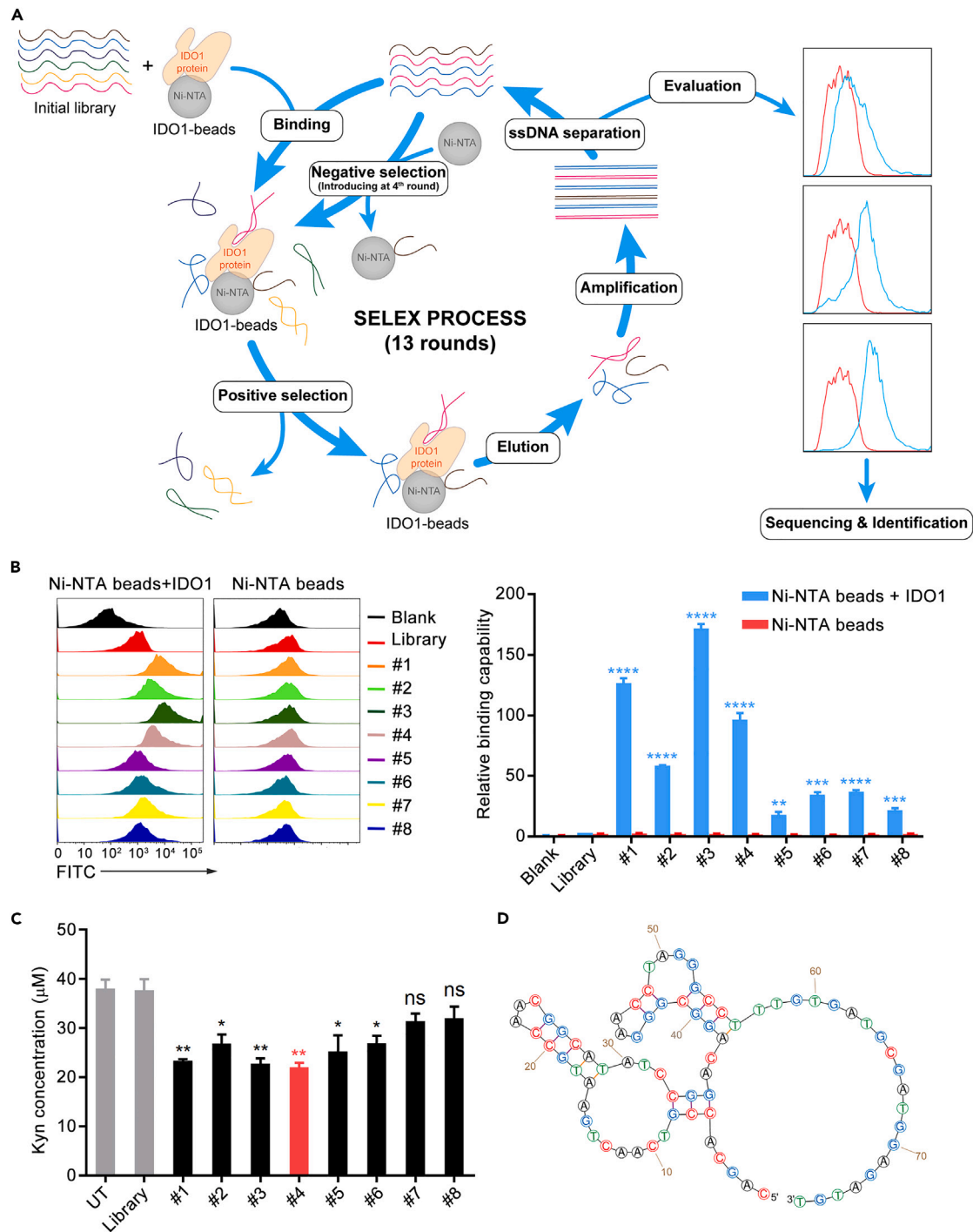https://doi.org/10.1016/j.isci.2023.107367

Figure 1. Selection of IDO1-targeting aptamer

(A) Schematic illustration of the protein-based SELEX process.

(B) Flow cytometry analysis of the target binding capability of aptamer candidates. Bare beads or 1 μg IDO1 coated beads were incubated with 250 nM aptamer candidates or initial library for 1 h. The mean fluorescence intensity (MFI) of aptamers was used to reflect the binding capacity. MFI of blank was set as 1. Statistical significance between aptamer candidates and the initial library was assessed by two-tailed unpaired Student's t test (n = 3, mean ± SEM, **p < 0.01, ***p < 0.001, ****p < 0.0001).

Figure 1. *Continued*

(C) Kyn level was evaluated by *in vitro* IDO1 enzyme activity assay to determine the inhibitory effect of aptamer candidates. A mixture of 20 μg/mL IDO1 protein and 500 nM aptamer candidates or initial library in 100 μL reaction buffer was set as the reaction system. Statistical significance between aptamer candidates and the initial library was assessed by two-tailed unpaired Student's *t* test (n = 3, mean $\pm$ SEM, ns means not significant, *p < 0.05, **p < 0.01).

(D) The predicted secondary structure of IDO-APT. Data in (B and C) are representative of three independent experiments.

with optimum inhibitory effect on IDO1, we selected IDO-APT from the pool of aptamer candidates by evaluating its impact on IDO1 enzyme activity. Subsequently, the binding affinity and specificity of IDO-APT to IDO1 were determined. Recognizing the challenge of aptamer internalization in cells, we introduced biomimetic mineralized nanoparticles (NPs) as a delivery tool. By conjugating IDO-APT with NPs, we investigated its function in primary T cells and mouse models. *In vitro* T cell culture assays demonstrated that IDO-APT reduced the proportion of T_{reg} cells and increased the expression of IFN-γ and TNF-α in CD8$^+$ T cells. The anti-tumor effects of IDO-APT were also examined in a mouse colon cancer CT26 syngeneic model. Our study reveals that IDO-APT effectively delays tumor growth and enhances immune response.

RESULTS

Screening of the IDO1-targeting DNA aptamer by protein-based SELEX

Firstly, we expressed and purified recombinant His-tagged mouse IDO1 protein using a prokaryotic system. To isolate aptamers, we employed a single-stranded DNA library to perform recombinant protein-based SELEX (Figure 1A). The single-stranded DNA library consisted of a 40-nucleotide random region flanked with two fixed 18-nucleotide primer binding regions, as shown in Figure S1A. Following 13 rounds of DNA aptamer selection, IDO1-targeting sequences were enriched from the ssDNA pool (Table S1; Figure S1B). Selected aptamers were identified through cloning and sequencing. Then the aptamer candidates from the 13th pool were subjected to the sequence alignment by ClustalX 2.1 (Figure S1C), and the eight most abundant sequences are listed in Table S2.

To evaluate the binding ability of aptamers to targets, we chemically synthesized the eight candidates and labeled them with fluorophores (FAM) at 5′ ends. Next, aptamer candidates were incubated with IDO1 protein-coated Ni-NTA magnetic beads, and the fluorescence intensity on the beads was analyzed by flow cytometry (Figure 1B). The first four aptamers (#1, #2, #3, and #4) with higher abundance among the eight candidates exhibited a stronger binding capability to IDO1 compared to the initial ssDNA library or other aptamers. And the binding affinity of these four aptamers against IDO1 was determined by incubating FAM-labeled aptamers at different concentrations with IDO1 protein-coated Ni-NTA magnetic beads (Figure S2A). Considering that the function of IDO1 primarily relies on its enzymatic activity, recombinant mouse IDO1 protein was used to conduct *in vitro* enzymatic assays to examine the inhibitory effect of these aptamer candidates on IDO1 activity. Colorimetric measurement of the IDO1 catalytic product revealed a significant reduction in Kyn levels upon the addition of several aptamers (Figure 1C). We further measured the IC$_{50}$ values to quantitatively compare the inhibitory effects of these aptamers toward IDO1 (Figure S2B). Additionally, an enzyme kinetic assay was performed to assess the inhibition constant (K_i) of IDO1 (Figure S2C). After comparison, candidate #4, one of the strongest inhibitors, emerged as a fine starting point (Figure S2D). Consequently, we designated this aptamer as IDO-APT and proceeded with further characterizations.

With the help of a nucleic acid structure analysis tool, the secondary structure prediction showed that IDO-APT contains two stem-loop structures (Figure 1D). Moreover, 3D-structure prediction and docking simulation (Figure S2E) suggested that nucleotides 42−44, 51−55, and 61−65 of IDO-APT potentially bind to amino acid residues 119−126, 259−263, and 301−309 of IDO1 protein.

IDO-APT specifically binds to mouse IDO1

To investigate the binding affinity of IDO-APT to IDO1, we incubated different concentrations of FAM-labeled IDO-APT or scrambled aptamer with IDO1 protein-coated Ni-NTA magnetic beads and analyzed fluorescence intensity by flow cytometry. As shown in Figure 2A, IDO-APT exhibits a strong binding affinity toward mouse IDO1 protein, with a dissociation constant (K_D) of 131 $\pm$ 9 nM (Figure 2A). Next, *in vitro* enzymatic assay was performed in the presence of serially diluted IDO-APT or scrambled aptamer to confirm the inhibitory effect of IDO-APT on IDO1. The result shows that IDO-APT inhibits the enzymatic activity of IDO1 in an IC$_{50}$ value of 1.38 μM. Furthermore, the electrophoretic mobility shift assay (EMSA) was employed to
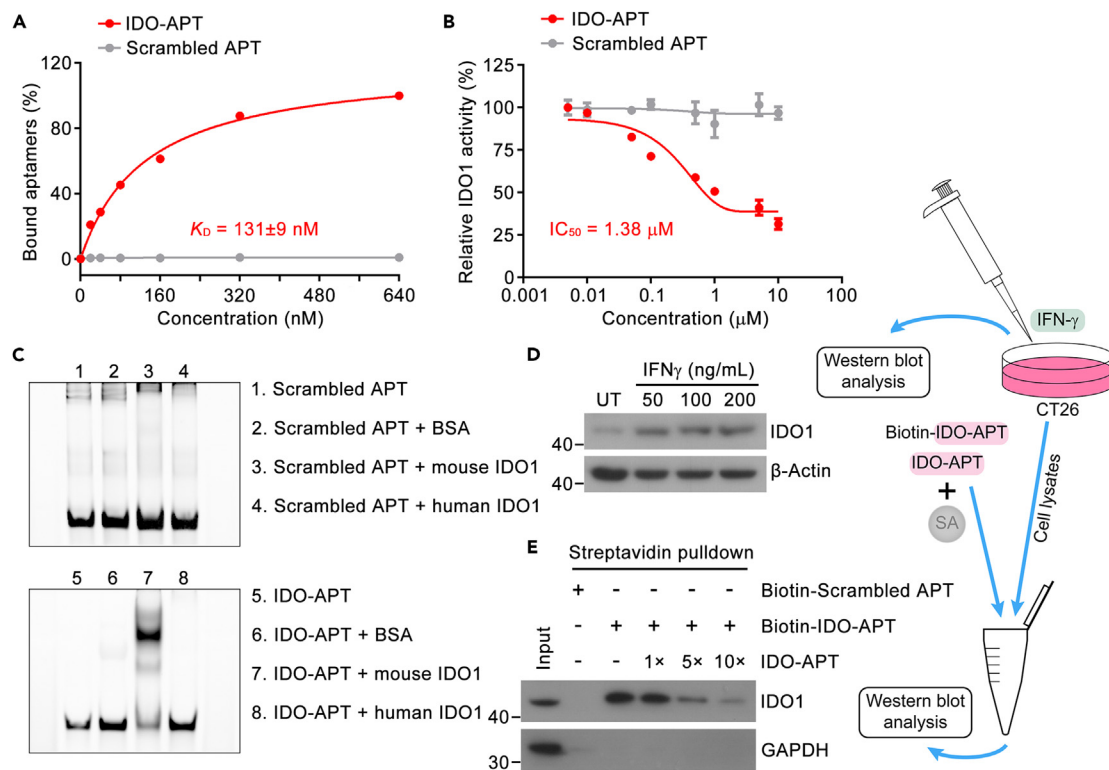
Figure 2. IDO-APT specifically binds with IDO1

(A) Dissociation constant (K_D) of IDO-APT measured by flow cytometry. Serially diluted IDO-APT or scrambled APT was incubated with 1μg IDO1 coated beads for 1 h. The MFI of IDO-APT in different concentrations was used to calculate the value of K_D. MFI of 640 nM IDO-APT was set as 100%.

(B) IC_{50} of IDO-APT was determined by in vitro IDO1 enzyme activity assay. A mixture of 20 μg/mL IDO1 protein and different concentrations of IDO-APT or scrambled APT in 100 μL reaction buffer was set as the reaction system. Kyn level of the group without aptamers was set as 100%.

(C) Mouse IDO1 protein retarded the migration of IDO-APT. A mixture of 100 nM IDO-APT and 1 mg/mL IDO1 protein was incubated at 4°C for 30 min, followed by native polyacrylamide gel electrophoresis.

(D) Western blotting determined the expression of IDO1 induced by IFN-γ in CT26 cells.

(E) Aptamer-mediated pull-down assay demonstrated specific binding between IDO-APT and IDO1 expressed in CT26 cells. 250 nM biotin-labeled IDO-APT or scrambled APT were used to capture IDO1 protein. IDO-APT without labeling (free IDO-APT) was added to compete with biotin-labeled IDO-APT. Data in (A–E) are representative of three independent experiments.

verify the targeting capability of IDO-APT. Following the incubation of IDO-APT with mouse IDO1 or control protein, gel electrophoresis was performed, and noticeable retardation in the electrophoretic mobility of the IDO-aptamer complex was observed (Figure 2C). In contrast, the migration of scrambled aptamer was not shifted by mouse IDO1 or control protein, indicating the specific binding between mouse IDO1 protein and IDO-APT.

To further validate the binding specificity of IDO-APT, we synthesized IDO-APT or scrambled aptamer tagged with 5′ biotin to perform the aptamer-mediated pull-down assay. Lysates of HEK293T cells that ectopically expressed IDO1-HA were incubated with these aptamers and precipitated by streptavidin beads. Protein binding on beads was then eluted and loaded on SDS-PAGE gel for electrophoresis. Western blot analysis showed that IDO-APT could successfully precipitate IDO1-HA (Figure S3A). In contrast, the scrambled aptamer could not bind to IDO1-HA. Moreover, an IDO1-specific protein band (about 45 kDa) was observed on the colloidal silver-stained SDS-PAGE gel (Figure S3B) and confirmed by mass spectrometry (MS) analysis. These results demonstrate the specific binding of IDO-APT with IDO1.

Considering the interference of the HA tag in this ectopic expression system, we next used an endogenous expression system with the CT26 cell line to perform the aptamer-mediated pull-down assay. Initially, we examined the expression of IDO1 in CT26 cells after being treated with different doses of IFN-γ. As shown in Figure 2D, IFN-γ at a concentration of 50 ng/mL led to sufficient IDO-1 expression. Then, the binding

between biotin-labeled IDO-APT and IDO-1 expressed in CT26 cells was demonstrated by pull-down assay, and the interaction between biotin-labeled IDO-APT and IDO-1could be disrupted in the presence of excess free IDO-APT (without biotin-label) (Figure 2E). These findings provide evidence that IDO-APT could successfully precipitate IDO1, and free IDO-APT competed with biotin-labeled IDO-APT in a dose-dependent manner.

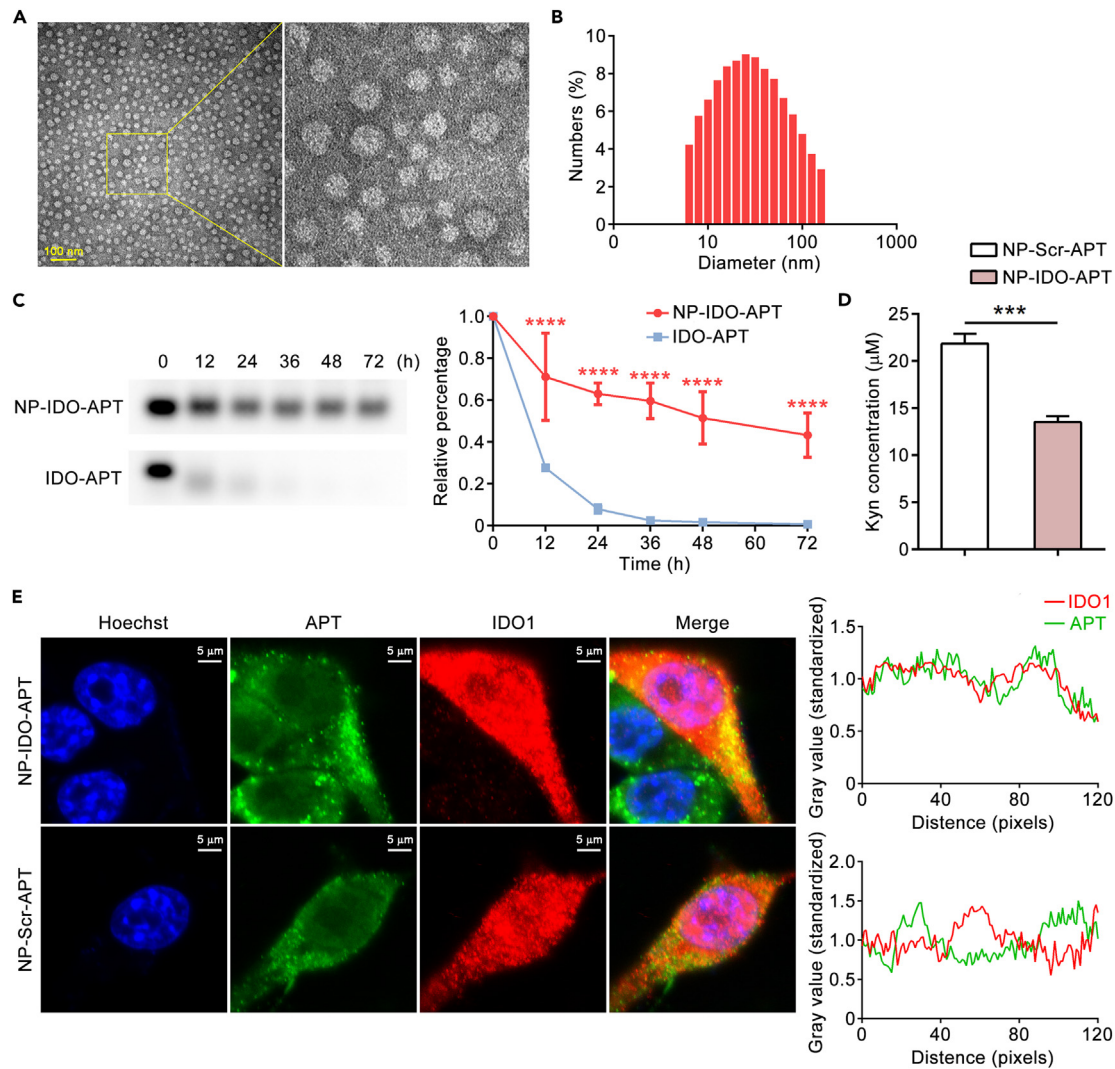## IDO-APT is internalized into cells by conjugating with nanoparticles

The aforementioned results demonstrate that IDO-APT effectively binds to mouse IDO1 and inhibits its activity. We next asked whether the aptamer has effects on cells. Generally, oligonucleotides like aptamers have limited ability to enter intracellular space, unless with the assistance of delivery carriers.[26] Protamine, a small polycationic peptide usually applied as the carrier for DNA or RNA delivery, was used to develop biomimetic biomineralization NPs in this study. By mixing aptamers with protamine in the presence of calcium salts, the aptamer-protamine nanocomplex spontaneously formed small-sized micelles. Different mass ratios of the aptamers and protamine were tested by agarose gel electrophoresis, and the ratio of IDO-APT to protamine at 4:1 displayed the optimum efficiency in assembling the aptamer-protamine complex (Figure S4A). Images of transmission electron microscopic (TEM) showed these NPs had regular spherical structures with a size between 10 and 50 nm (Figure 3A). In line with the TEM images, the average size and surface charge of IDO-APT, as determined by dynamic light scattering (DLS), were 60.3 nm and 1.44 mV, respectively (Figure 3B), suggesting the formation of NP-IDO-APT is stable and uniform.

Next, we examined the uptake of NP-conjugated IDO-APT (hereafter termed as NP-IDO-APT) in CT26 cells by confocal microscopy. As expected, obvious fluorescent signals of IDO-APT were observed in the intracellular space after incubating CT26 cells with 5' FAM-labeled NP-IDO-APT, whereas no fluorescent signals were detected in the bare aptamer incubation system, which demonstrated that NPs facilitated the entrance of IDO-APT to the cytoplasm (Figure S4B). We further compared the stability of NP-IDO-APT and bare aptamer in physical conditions by incubating them with 10% fetal bovine serum (FBS) for different time periods (0–72 h) at 37°C. As shown in Figure 3C, by conjugating with NPs, IDO-APT can stably exist in 10% FBS with a half-life of 48 h, while the band corresponding to bare IDO-APT quickly decreased with a half-life of less than 12 h. Thus, aptamer-protamine nanocomplex protected IDO-APT from degradation and prolonged its half-life.

Considering the introduction of NPs may influence the binding ability and inhibition effect of IDO-APT toward IDO1, we performed a cell-based IDO1 activity assay to determine the inhibitory effect of NP-IDO-APT on IDO1. As shown in Figure 3D, the level of Kyn in the culture medium was reduced when IFN-γ treated CT26 cells were applied with NP-IDO-APT for 24 h. Meanwhile, the expression level of IDO1 in CT26 cells remained stable after being administrated with NP-IDO-APT, NPs loaded with scrambled aptamer (hereafter termed as NP-Scr-APT), or NPs alone (Figure S4C). Subsequently, we evaluated the co-localization of IDO-APT with IDO1 by immunofluorescence assays (Figure 3E). The result revealed that IDO-APT partially colocalized with IDO1, by comparison, the colocalizing signal was barely seen in the NP-Scr-APT group, indicating the specific interaction of IDO-APT with IDO1 protein. Besides, the cytotoxicity of NP-IDO-APT was examined in CT26 cells. The growth of CT26 cells was monitored using a CCK-8 assay, and the proliferation of CT26 cells was unaffected after the administration of NP-IDO-APT, NP-Scr-APT, or NPs (Figure S4D). Apoptotic cell death of CT26 cells was also analyzed by flow cytometry, and the application of these treatments had no significant effect on the apoptosis of CT26 cells (Figure S4E). Above all, NPs enhanced the stability of IDO-APT and facilitated the internalization of IDO-APT without obvious cytotoxicity. Moreover, IDO-APT is able to bind IDO1 and inhibit its activity at the cellular level after conjugating NPs.

IDO-APT inhibits T_{reg} cells and promotes the activity of effector T cells

High levels of IDO1 in the tumor microenvironment promote T_{reg} cells and induce T cell anergy.[27] Previous reports have shown that IDO1 inhibition could reverse the effect of dendritic cells (DCs) to promote T_{reg} cell conversion and enhance the ability of DCs to activate T cells.[28,29] We then examined if IDO-APT treatment led to suppression of T_{reg} cells and enhancement of effector T cell function by in vitro T cell culture assays. Specifically, we isolated lymphocytes from the spleen of BALB/c mice and treated them with NP-IDO-APT, NP-Scr-APT, or NPs. After culturing for 6 days, the percentage of T_{reg} cells ($CD4^+$ $CD25^+$ $Foxp3^+$) was measured by flow cytometry. Treatment with NP-IDO-APT reduced the proportion of $CD25^+$ $Foxp3^+$ cells in $CD4^+$ T cells compared with NP-Scr-APT or NPs treatment (Figures 4A and S5A). Next, we stimulated

Figure 3. Characterization of mineralized nanoparticle conjugated IDO-APT

(A) TEM image of NP-IDO-APT. Scale bars = 100 nm.

(B) Size distribution of NP-IDO-APT determined by DLS.

(C) Gel electrophoresis shows the stability of NP-IDO-APT at different times. RPMI 1640 containing 10% FBS was mixed with 100 nM FAM-labeled NP-IDO-APT or IDO-APT alone. The grayscale value of IDO-APT was calculated (right panel), and the grayscale value of IDO-APT that unincubated was set as 1 (n = 3, mean ± SEM, ****p < 0.0001).

(D) Cell-based IDO1 activity assay was performed to detect the Kyn level of the culture medium. CT26 cells were supplemented with 200 nM NP-IDO-APT or NP-Scr-APT and cultured for 24 h (n = 3, mean ± SEM, ***p < 0.001).

(E) Colocalization of IDO-APT and IDO1 protein was determined by immunofluorescence assay. IFN-γ treated CT26 cells were incubated with 200 nM NP-IDO-APT or NP-Scr-APT for 12 h. Statistical analysis of the fluorescence signal between aptamer (green) and IDO1 (red) was shown in the right panel. Scale bars = 5 μm. Statistical significance was assessed by two-way ANOVA (C) followed by Tukey's multiple comparisons test or two-tailed unpaired Student's *t* test (D). Data in (A–E) are representative of three independent experiments.

these cultured lymphocytes with phorbol ester (PMA), ionomycin, and protein transport inhibitor cocktail to evaluate the intracellular cytokine levels of T cells. After treatment with NP-IDO-APT, CD8$^+$ T cells produced more TNF-α and IFN-γ, while this effect was not observed in NP-Scr-APT or NPs treatment (Figures 4B, 4C, S5B, and S5C).

To comprehensively illustrate IDO-APT's effects on T cell function, we performed an RNA sequencing assay of activated lymphocytes that were treated by NP-IDO-APT or NP-Scr-APT. Gene Ontology (GO) enrichment analysis identified pathways related to cytokine activity enriched in NP-IDO-APT-treated
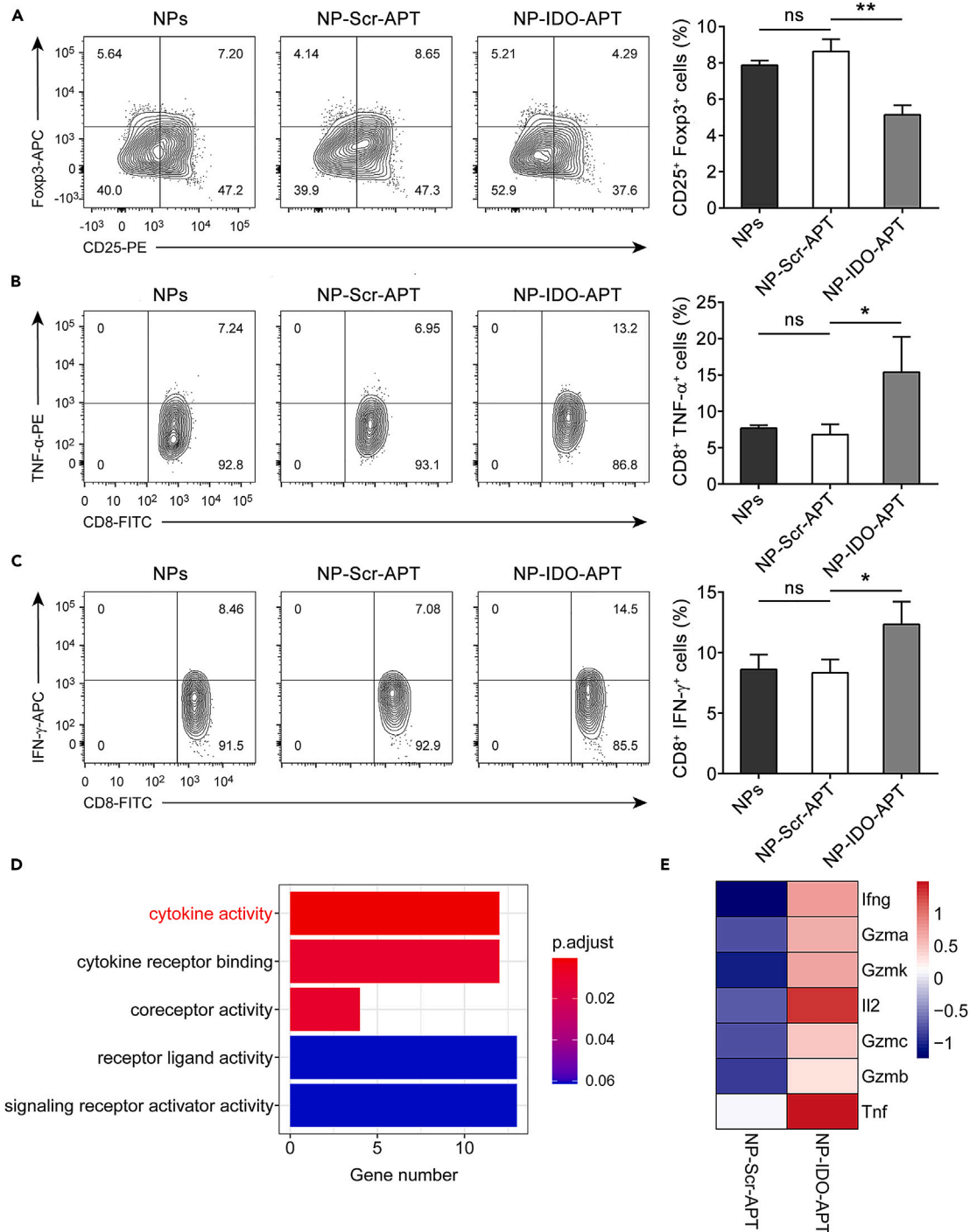
Figure 4. IDO-APT promotes T cell function *in vitro*

Mouse spleen lymphocytes were cultured *in vitro* with 100 nM NPs, NP-Scr-APT, or NP-IDO-APT for 6 days, followed by flow cytometry analysis and RNA sequencing.

(A) The percentage of CD25$^+$ Foxp3$^+$ cells was determined by flow cytometry (n = 4 cell cultures, mean $\pm$ SEM, ns means not significant, **p < 0.01).

(B) Flow cytometric analysis of TNF-α expression in CD8$^+$ T lymphocytes (n = 3 cell cultures, mean $\pm$ SEM, ns means not significant, *p < 0.05).

(C) Flow cytometric analysis of IFN-γ expression in CD8$^+$ T lymphocytes (n = 3 cell cultures, mean $\pm$ SEM, ns means not significant, *p < 0.05).

(D) GO enrichment analysis identified pathways in lymphocytes treated with NP-IDO-APT.

Figure 4. *Continued*

(E) Heatmap of the RNA-seq results related to T cell effector factors. The expression of each gene from the different groups was scaled by Z score. Statistical significance was assessed by one-way ANOVA (A, B, and C) followed by Tukey's multiple comparisons test. Data in (A, B, and C) are representative of three independent experiments.

lymphocytes (Figure 4D). As shown in Figure 4E, T cell effector factors such as *Ifng*, *Gzmb*, *Tnf*, and *Il2* were upregulated in lymphocytes following NP-IDO-APT treatment compared with NP-Scr-APT exposure. Together, we demonstrate that IDO-APT restricts the production of T_{reg} cells and elevates the effector function of T cells.

The immunostimulatory effect of IDO-APT on T cells is mediated by DCs

Because the lymphocytes derived from the spleen consist of different immune cells, it is still necessary to figure out which component mediates the activation of T cell function in the presence of IDO-APT. Since DCs is the main cells that expressed high levels of IDO1 among tumor-infiltrating lymphocytes (TILs), while T cells barely express IDO1, we hypothesized that IDO-APT activates T cells by targeting DCs. To determine the role of DCs in IDO-APT-treated T cells, we established a coculture system (Figure 5A). As shown in Figures 5B and 5C, DCs were induced from bone marrow cells (BMs) and expressed IDO1 under IFN-γ treatment. The IFN-γ/LPS-stimulated BMDCs and CD3$^+$ T cells were subsequently cocultured for 6 days applied with NP-IDO-APT, NP-Scr-APT, or NPs, and the intracellular cytokine levels of T cells were detected by flow cytometry. Compared with NP-Scr-APT or NPs treatment, CD8$^+$ T cells exhibit a higher level of TNF-α and IFN-γ in the presence of NP-IDO-APT, whereas this effect was not seen when CD3$^+$ T cells were cultured alone (Figures 5D, 5E, S6A, and S6B).

The expression of IDO1 in IFN-γ/LPS-stimulated DCs was also confirmed by immunofluorescence assays, and the colocalizing signal of IDO-APT and IDO1 was observed as well (Figure 5F). Previous studies have shown that inhibiting IDO1 in DCs leads to a stimulatory effect on T cells.[30,31] Hence, the reduction of Kyn levels in NP-IDO-APT-treated DCs, shown in Figure 5G, supports our hypothesis that IDO-APT inhibits IDO1 expressed in DCs and enhances the function of CD8$^+$ T cells.

IDO-APT suppresses tumor growth in CT26 murine syngeneic model

The immunostimulatory effect of IDO-APT on lymphocytes prompted us to investigate its effect *in vivo*. In the CT26 murine syngeneic tumor model, BALB/c mice were subcutaneously inoculated with CT26 cells. The treatment was started once inoculated tumors reached a size of ∼50 mm^3. NP-IDO-APT, NP-Scr-APT, and NPs were administered at a dosage of 1.5 mg/kg by s.c. injection directly to the tumor on day 6, day 9, and day 12 after seeding (Figure 6A). The tumor size monitoring data showed that mice administered with NP-IDO-APT exhibited retarded tumor growth compared with mice treated with NP-Scr-APT or NPs (Figures 6B and 6C). NP-IDO-APT administration induced over 50% tumor weight reduction compared with the group of NP-Scr-APT administration (Figures 6D and 6E).

To further confirm the tumor-suppressive effect of IDO-APT, we then treated the mice with three different dosages of NP-IDO-APT. As shown in Figures 6F and 6G, in line with the aforementioned results, the intermediate dosage of NP-IDO-APT (1.5 mg/kg) hindered CT26 tumor growth, meanwhile, the high dosage of NP-IDO-APT (2.5 mg/kg) greatly inhibited tumor growth in a stronger way, and the low dosage of NP-IDO-APT (0.5 mg/kg) only showed moderate tumor control, compared with the group that treated with NP-Scr-APT or NPs. Consistently, the high dosage of NP-IDO-APT also significantly prolonged the survival of the tumor-bearing mice, whereas the low dosage of NP-IDO-APT barely changed the survival of tumor-bearing mice, compared with the NPs or NP-Scr-APT administration group (Figure S7). These results suggest that IDO-APT impeded tumor growth and extended survival in a dosage-dependent manner.

Considering the modulatory role of IDO1 on the adaptive immune system in tumor microenvironment, we supposed that the inhibitory effect of IDO-APT on CT26 tumors was mediated by lymphocytes instead of direct cytotoxicity. To test this hypothesis, we examined the anti-tumor effect of IDO-APT in immune-deficient non-obese diabetic (NOD)/severe combined immunodeficiency (SCID) mice. Under the same treatment as BALB/c mice, NOD/SCID mice bearing CT26 tumors did not show significant differences in tumor growth (Figures 6H and 6I). This result indicated that tumor control of IDO-APT is in an immune cell-dependent manner.
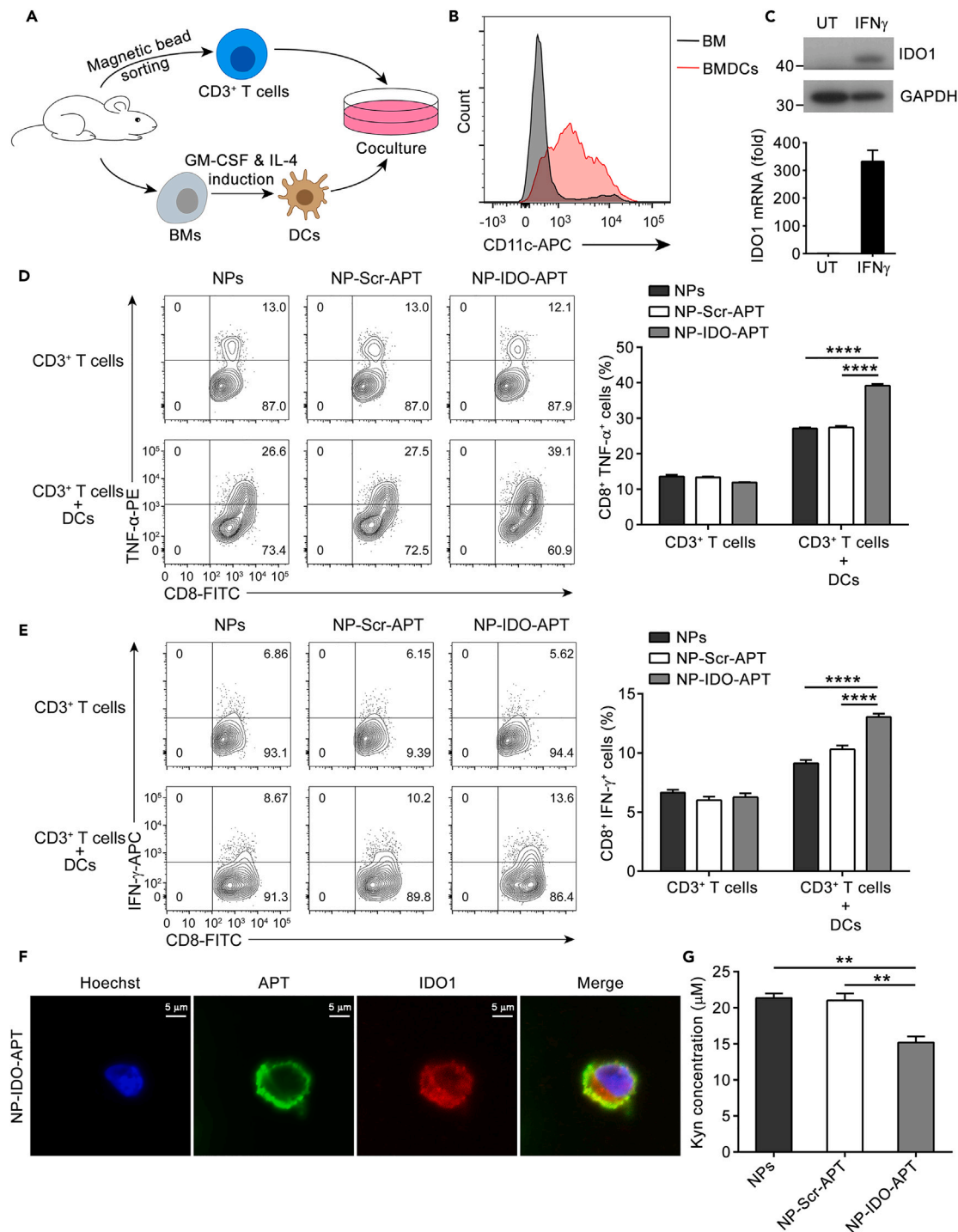
Figure 5. IDO-APT inhibits IDO1 activity in DCs to promote T cell activation

DCs and CD3^{+} T cells at the ratio of 1:10 were cocultured *in vitro* with 100 nM NPs, NP-Scr-APT, or NP-IDO-APT for 6 days, followed by flow cytometry analysis.

(A) Schematic illustration of DCs & T cells coculture assay.

(B) BMDCs induced from BMs were analyzed by flow cytometry. CD45 and CD11b were used to indicate the proportion of DCs.

(C) The mRNA and protein expression of IDO1 in DCs were determined after being treated with 50 ng/mL IFN-γ for 24 h, mRNA level of IFN-γ-untreated DCs was set as 1.

(D) Flow cytometric analysis of TNF-α expression in CD8^{+} T cells (n = 3 cell cultures, mean ± SEM, ****p < 0.0001).

Figure 5. Continued

(E) Flow cytometric analysis of IFN-γ expression in CD8$^+$ T cells (n = 3 cell cultures, ****p < 0.0001).

(F) The internalization of IDO-APT in DCs was determined by immunofluorescence assay. IFN-γ treated DCs were incubated with 200 nM NP-IDO-APT for 12 h. Scale bars = 5 μm.

(G) Cell-based IDO1 activity assay was performed to detect the Kyn level of the culture medium. DCs were treated with 200 nM NPs, NP-Scr-APT, or NP-IDO-APT and cultured for 24 h (n = 3, **p < 0.01). Statistical significance was assessed by one (G) or two (D and E)-way ANOVA followed by Tukey's multiple comparisons test. Data in (B–G) are representative of two independent experiments.

Given that IDO-APT exhibits the ability of tumor control in mice, we next determined whether this effect is via the inhibition of IDO1. The endogenous IDO1 expression in CT26 cells was knocked down by the use of short hairpin RNA (shRNA), and the knockdown efficiency of IDO1 was confirmed by RT-PCR and Western blot (Figure S8). We subsequently detected the anti-tumor effect of IDO-APT in BALB/c mice bearing IDO1 knockdown CT26 tumors. As shown in Figures 6J and 6K, the overall tumors with defect IDO1 exhibit a re-tarding growth, and the tumor suppressive effect of IDO-APT was impaired in IDO1 knockdown CT26 tumors, compared with IDO1 sufficient tumors. Thus, IDO1 is the essential factor to achieve the anti-tumor of IDO-APT.

Furthermore, these treatments were well tolerated by the mice, as no abnormal physical effects were observed during the experimental period. The body weight of mice was stable in each group during admin-istration (Figure S9A). In addition, after the last treatment, levels of alanine aminotransferase (ALT) and aspartate aminotransferase (AST) in the plasma were determined to assess liver function, and levels of blood urea nitrogen (BUN) and creatinine (CREA) in the plasma were tested to evaluate renal function. The result of these blood biochemical indexes showed no measurable liver or renal toxicities (Figure S9B).

Together, these findings suggest that IDO-APT suppresses tumor growth without observable toxicity, and this effect relies on the existence of intact lymphocytes.

IDO-APT inhibits *in vivo* IDO1 activity and enhances anti-tumor immunity

The *in vitro* inhibitory effect of IDO-APT on IDO1 raised the possibility that the administration of IDO-APT may result in the suppression of IDO1 activity in tumor tissue. We then detected *in vivo* IDO1 enzyme ac-tivity which was indicated by measuring the consumption of Trp and the production of Kyn. Two days after the last administration, we obtained the plasma and tumors of tumor-bearing mice and performed liquid chromatography-tandem MS (LC-MS/MS). As shown in Figure 7A, ratios of Kyn/Trp in both plasma and tu-mors were significantly reduced after being treated with NP-IDO-APT. To exclude the influence of IDO1 expression, we examined mRNA and protein levels of IDO1 in CT26 tumors and found no significant change among the groups that were treated with NP-IDO-APT, NP-Scr-APT, or NPs (Figure S10). This result suggests that IDO-APT inhibits IDO1 activity without affecting its expression level.

We next analyzed the population of tumor tissues infiltrated lymphocytes by flow cytometry. As shown in Figure 7B, there were more TILs in tumors that received NP-IDO-APT treatment, as indicated by the elevated count of CD45$^+$ cells. NP-IDO-APT administration also increased the proportion of CD8$^+$ T cells in TILs (Figure 7C). TNF-α and IFN-γ expression of CD8$^+$ T cells in tumors were significantly increased after being treated with NP-IDO-APT (Figures 7D, 7E, S11A, and S11B). Fewer CD4$^+$ CD25$^+$ Foxp3$^+$ cells were observed in TILs, indicating the inhibition of T$_{reg}$ cell induction in NP-IDO-APT treated tumors (Fig-ures 7F and S11C).

It has been reported that tumor-associated macrophages (TAMs) and myeloid-derived suppressor cells (MDSCs) in the tumor microenvironment elevate the expression of IDO1 and exhibit immunosuppressive activities.[32] We, therefore, estimated the abundance of those cells. As shown in Figures 7G and 7I, the numbers of TAMs (CD45$^+$ CD11b$^+$ F4/80$^+$) and granulocytic MDSCs (G-MDSCs, CD45$^+$ CD11b$^+$ Ly6G$^+$) were significantly reduced in tumors administered with NP-IDO-APT. In contrast, there were no significant differences among all treatments in the numbers of monocytic MDSCs (M-MDSCs) defined by CD45$^+$ CD11b$^+$ Ly6C$^+$ (Figures 7H and S11D).

In brief, our data demonstrate that NP-IDO-APT treatment induces a more immunoreactive tumor micro-environment, and this effect is likely mediated by the inhibition of IDO1 activity, leading to tumor suppres-sion and prolonged survival.
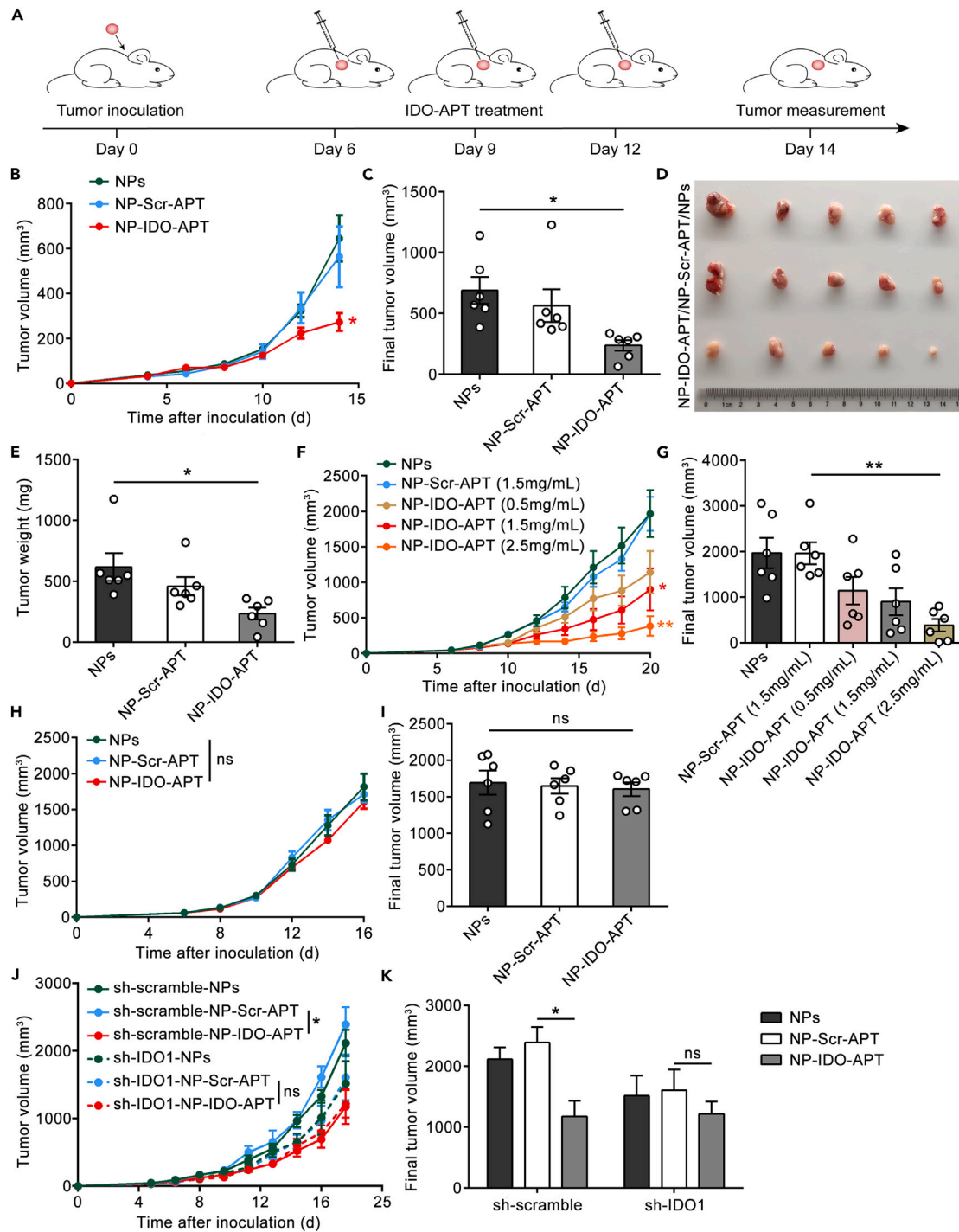
Figure 6. IDO-APT suppresses tumor growth in the CT26 tumor-bearing mouse model

(A) Schematic illustration of the tumor model and treatment. Female BALB/c mice bearing CT26 tumors of ~50 mm³ received 1.5 mg/kg NPs, NP-Scr-APT, or NP-IDO-APT at day 6, day 9, and day 12, by s.c. injection directly into the tumor. Tumor volumes were measured every 2 days.

(B) IDO-APT inhibited tumor growth (n = 6 mice, mean ± SEM, *p < 0.05).

(C) Volumes of final excised tumors for each treatment were recorded (n = 6 mice, mean ± SEM, *p < 0.05).

(D) Representative images of final excised tumors (n = 5 mice).

(E) Tumors were weighed after sacrifice (n = 6 mice, mean ± SEM, *p < 0.05).

Figure 6. Continued

(F) Female BALB/c mice bearing CT26 tumor of ~50 mm^3 received three different dosages of NP-IDO-APT and were treated the same way as described above. Tumor volumes were recorded every 2 days (n = 6 mice, mean ± SEM, ns means not significant, *p < 0.05, **p < 0.01).

(G) Volumes of final excised tumors for each treatment (n = 6 mice, mean ± SEM, ns means not significant, **p < 0.01).

(H) Female NOD/SCID mice bearing CT26 tumors of ~50 mm^3 were treated the same way as described above. Tumor volumes were recorded every 2 days (n = 6 mice, mean ± SEM, ns means not significant).

(I) Volumes of final excised tumors for each treatment in NOD/SCID mice were measured (n = 6 mice, mean ± SEM, ns means not significant).

(J) Female BALB/c mice bearing IDO1-deficient CT26 tumors or IDO1-sufficient CT26 tumors of ~50 mm^3 were treated the same way as described above. Tumor volumes were recorded every 2 days (n = 4 mice, mean ± SEM, ns means not significant, *p < 0.05).

(K) Volumes of final excised tumors for each treatment (n = 4 mice, mean ± SEM, ns means not significant, *p < 0.05). Statistical significance was assessed by one (C, E, G, and I) or two (B, F, H, J, and K)-way ANOVA followed by Tukey's multiple comparisons test. Data in (B–K) are representative of two independent experiments.

DISCUSSION

Cancer immunotherapy has become an increasing focus of cancer therapy for years. IDO1, a well-known immunoregulatory factor, is widely expressed in a number of cancers and maintains immune tolerance, which makes it become a valuable therapeutic target.[33] Aiming to develop the approach in cancer immunotherapy, numerous inhibitors of IDO1, mainly small molecular inhibitors, have been generated.[34] However, the frustrating clinical development of these available IDO1 inhibitors motivated us to seek alternative strategies. In this research, we reported a novel IDO1-targeting DNA aptamer, IDO-APT, and demonstrated that IDO-APT effectively inhibits IDO1 activity and suppresses tumor growth.

A purified recombinant His-tagged mouse IDO1 protein was used to perform the SELEX procedure from the beginning, and we obtained eight aptamer candidates expecting to isolate a functional aptamer that antagonizes IDO1. In the following study, the exploration was based on aptamer candidate #4, and it indeed performed well in subsequent cell-based and *in vivo* assays. Nevertheless, it is acknowledged that other aptamer candidates may also have potential activities. Further investigation could explore the function of these candidates and determine if any of them possess a stronger anti-tumor effect.

As yet, the targets of aptamers are mainly membrane proteins, whereas IDO1 is located in the cytoplasm. Owing to charge repulsion and size, most aptamers are subject to resistance to cellular uptake.[35] Because of the presence of space obstacles, the internalization ability is very important for *in vivo* applications of IDO-APT. To address the targetable delivery of IDO-APT, we developed a biomimetic biomineralization NP delivery system with a protamine-aptamer complex core for aptamer protection and an amorphous calcium hydrogen phosphate ion shell covered in the outer layer to aid the cellular uptake of aptamers and transfer to the cytoplasm. This NP protects aptamers from degradation and efficiently transfers IDO-ATP through the cell membrane to target the cytoplasm-located IDO1 protein. Through endocytosis, mineralized NPs are wrapped in endosomes and enter into cells.[36] After that, mature endosomes acidify and fuse with lysosomes, NPs conduct lysosomes escape via the proton sponge effect, by which NPs disintegrate and release aptamers into the cytoplasm.[37,38] Protamine is a cationic polypeptide rich in arginine residues, which can form stable complexes with negatively charged nucleic acids.[39] According to these previous reports, we assumed that NPs internalized via the endo-lysosomal route and released to the cytoplasm through endosomal escape. Because of the absence of active targeting moieties, the cellular uptake of NPs seemed nonspecific, we had to administrate NP-IDO-APT by means of intra-tumoral injection. For the further application and translation of IDO-APT, the targeted delivery vehicles should be employed in future studies.

In a previous report, it was shown that IDO1 expressed in DCs promotes T$_{reg}$ cell differentiation and suppresses T cell responses.[40] Accordingly, our *in vitro* experiments demonstrated that culturing lymphocytes with IDO-APT decreases the proportion of T$_{reg}$ cells and boosts the function of CD8$^+$ T cells. While, due to the complex composition of lymphocytes, we do not ascertain which immune cells exert their effect on this process. Considering that DCs are one of the predominant immune cells expressing IDO1 and that IDO1 activation in DCs suppresses T cell responses, inhibiting IDO1 in DCs could enhance the immune responses of T cells.[41–43] Hence, we isolated CD3$^+$ T cells and bone marrow-derived DCs to proceed *in vitro* coculture assay and demonstrated that IDO-APT inhibits IDO1 activity in DCs to mediate T cell activation.

The anti-tumor effect of IDO-APT was also tested in both immunosufficient BALB/c mice and immunodeficient NOD/SCID mice. Significant tumor control was observed in BALB/c mice but not NOD/SCID mice
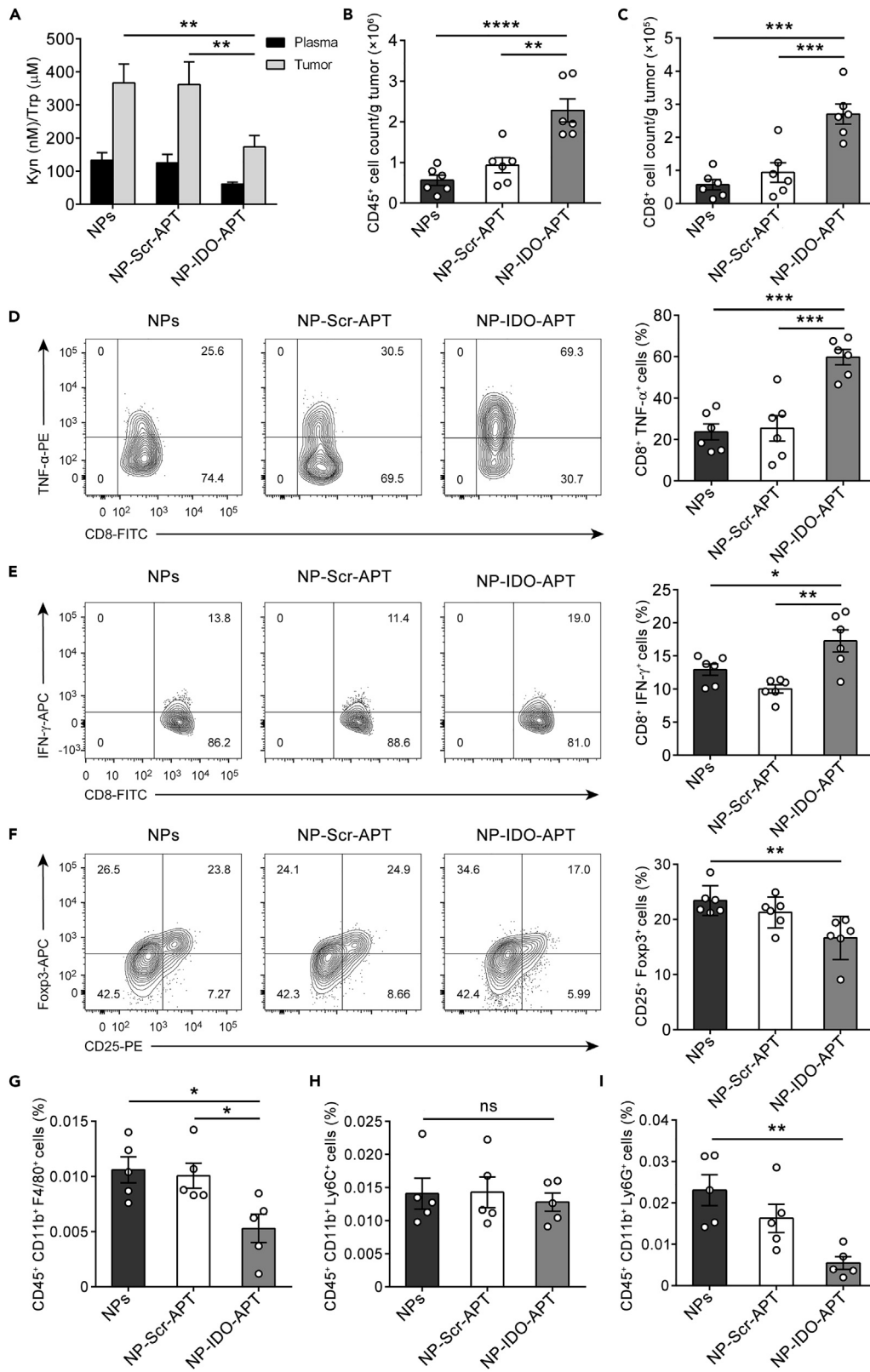
Figure 7. IDO-APT inhibits IDO1 activity and promotes anti-tumor immune response in tumor-bearing mice

Female BALB/c mice bearing CT26 tumors receiving the same treatment as Figure 6A were harvested tumor tissue and plasma two days after the last injection for further determination.

(A) Ratios of Kyn (nM)/Trp (μM) in mouse plasma and tumor tissue were determined by LC−MS/MS (n = 6 mice, mean ± SEM, **$p < 0.01$).

(B) Quantifying the counts of tumor-infiltrating CD45$^+$ cells by flow cytometry (n = 6 mice, mean ± SEM, **$p < 0.01$, ****$p < 0.0001$).

(C) Quantifying the counts of tumor-infiltrating CD8$^+$ T cells by flow cytometry (n = 6 mice, mean ± SEM, ***$p < 0.001$).

(D) Flow cytometric analysis of TNF-α expression in CD8$^+$ T cells (n = 6 mice, mean ± SEM, ***$p < 0.001$).

(E) Flow cytometric analysis of IFN-γ expression in CD8$^+$ T cells (n = 6 mice, mean ± SEM, *$p < 0.05$, **$p < 0.01$).

(F) The percentage of CD25$^+$ Foxp3$^+$ cells gated in CD4$^+$ lymphocytes was analyzed by flow cytometry (n = 6 mice, mean ± SEM, **$p < 0.01$).

(G) The percentage of CD11b$^+$ F4/80$^+$ cells gated in CD45$^+$ lymphocytes was analyzed by flow cytometry (n = 5 mice, mean ± SEM, *$p < 0.05$).

(H) The percentage of CD11b$^+$ Ly6C$^+$ cells gated in CD45$^+$ lymphocytes was analyzed by flow cytometry (n = 5 mice, mean ± SEM, ns means not significant).

(I) The percentage of CD11b$^+$ Ly6G$^+$ cells gated in CD45$^+$ lymphocytes was analyzed by flow cytometry (n = 5 mice, mean ± SEM, **$p < 0.01$). Statistical significance was assessed by one (B–I) or two (A)-way ANOVA followed by Tukey's multiple comparisons test. Data in (A–I) are representative of two independent experiments.

that received NP-IDO-APT treatment, suggesting IDO-APT relies on the existence of intact lymphocytes to achieve its tumor suppressive effect. Indeed, immunological analysis of TILs revealed that NP-IDO-APT treatment leads to an increase in functional CD8$^+$ T cells and a decrease in T$_{reg}$ cells, compared with the control group. In addition, the decreased proportion of TAMs and G-MDSCs further supported the formation of a more immunoreactive microenvironment in tumors that are being treated with NP-IDO-APT.

To address whether the anti-tumor effect of IDO-APT depends on IDO1 expression in cancer cells, we employed shRNA to knock down IDO1 expression. Unlike the significant tumor control effect of IDO-APT in IDO1 sufficient CT26 tumors, the growth of IDO1 knockdown CT26 tumors showed only a slight reduction (no significant) after being administrated with NP-IDO-APT, compared with the control groups (NPs or NP-Scr-APT), suggesting that IDO1 expression is essential for IDO-APT to suppress tumors. Consistent with previous studies that IDO1 knockout induced the suppression of tumor growth,[44,45] IDO1 knockdown CT26 tumors exhibited a hindering growth. Meanwhile, it is possible that other immune cells in the tumor microenvironment with intact IDO1, especially DCs, contribute to the slight anti-tumor effect of IDO-APT in IDO1 knockdown CT26 tumors bearing mice. Future studies employing systematic and conditional knockout mice of IDO1 could provide further insights into the anti-tumor effect of IDO-APT.

Taken together, IDO-APT is the first IDO1-targeting aptamer that exhibits the immune enhancement role in the tumor microenvironment and leads to tumor suppression. Our data represent a new approach to the development of IDO1 inhibitors which may be exploited as a potential immunotherapeutic strategy. Considering the combination of chemotherapy and immunotherapy has become an attractive approach to improve cancer therapy,[46,47] investigating the synergistic effects of IDO1-APT with other chemotherapeutic agents would be valuable and should be explored in future investigations.

Limitations of the study

It also should be noted that the aptamer we obtained contains primer binding regions at both ends. Concern to expand the application and reduce the synthesis costs, shortening and optimizing the length of aptamers is regarded as a valid means. We once attempted to remove the primer regions of IDO-APT, but the binding ability of truncated IDO-APT was impaired (Figure S12). Hence, the full-length IDO-APT was used in this study. Currently, the strategy of aptamer truncation basically refers to the secondary structure or primer regions of aptamers and predicted binding domains of the aptamer-target complex.[48] For the future application of IDO-APT, truncation based on 3D structure prediction and docking simulation could be employed to identify regions that are crucial for target binding while eliminating non-essential sequences.

STAR★METHODS

Detailed methods are provided in the online version of this paper and include the following:

SUPPLEMENTAL INFORMATION

Supplemental information can be found online at https://doi.org/10.1016/j.isci.2023.107367.

AUTHOR CONTRIBUTIONS

Z.Z. and Y.Yin conceived the study and designed experiments. Z.Z. and Z.Y. performed the experiments and analyzed the data. C.Z. contributed to nanoparticle construction. Z.H. and Z.J. assisted in experiments. J.G. performed tumor inoculation. Y.Yuan performed mass spectrometry analysis. X.C. performed blood biochemical analysis. Y.J. provided technical assistance. Y.Yin supervised this project. Z.Z. and Y.Yin wrote the manuscript.

DECLARATION OF INTERESTS

The authors declare that they have no competing interests.

REFERENCES

1. Kraehenbuehl, L., Weng, C.H., Eghbali, S., Wolchok, J.D., and Merghoub, T. (2022). Enhancing immunotherapy in cancer by targeting emerging immunomodulatory pathways. Nat. Rev. Clin. Oncol. *19*, 37–50. https://doi.org/10.1038/s41571-021-00552-7.

2. Sadreddini, S., Baradaran, B., Aghebati-Maleki, A., Sadreddini, S., Shanehbandi, D., Fotouhi, A., and Aghebati-Maleki, L. (2019). Immune checkpoint blockade opens a new way to cancer immunotherapy. J. Cell. Physiol. *234*, 8541–8549. https://doi.org/10.1002/jcp.27816.

3. Prendergast, G.C., Smith, C., Thomas, S., Mandik-Nayak, L., Laury-Kleintop, L., Metz, R., and Muller, A.J. (2014). Indoleamine 2,3-dioxygenase pathways of pathogenic inflammation and immune escape in cancer. Cancer Immunol. Immunother. *63*, 721–735. https://doi.org/10.1007/s00262-014-1549-4.

4. Takikawa, O., Yoshida, R., Kido, R., and Hayaishi, O. (1986). Tryptophan degradation in mice initiated by indoleamine 2,3-dioxygenase. J. Biol. Chem. *261*, 3648–3653.

5. Ferns, D.M., Kema, I.P., Buist, M.R., Nijman, H.W., Kenter, G.G., and Jordanova, E.S. (2015). Indoleamine-2,3-dioxygenase (IDO) metabolic activity is detrimental for cervical cancer patient survival. OncoImmunology *4*, e981457. https://doi.org/10.4161/2162402X.2014.981457.

6. Munn, D.H., Sharma, M.D., Baban, B., Harding, H.P., Zhang, Y., Ron, D., and Mellor, A.L. (2005). GCN2 kinase in T cells mediates proliferative arrest and anergy induction in response to indoleamine 2,3-dioxygenase. Immunity *22*, 633–642. https://doi.org/10.1016/j.immuni.2005.03.013.

7. Metz, R., Rust, S., Duhadaway, J.B., Mautino, M.R., Munn, D.H., Vahanian, N.N., Link, C.J., and Prendergast, G.C. (2012). IDO inhibits a tryptophan sufficiency signal that stimulates mTOR: A novel IDO effector pathway targeted by D-1-methyl-tryptophan. OncoImmunology *1*, 1460–1468. https://doi.org/10.4161/onci.21716.

8. Mezrich, J.D., Fechner, J.H., Zhang, X., Johnson, B.P., Burlingham, W.J., and Bradfield, C.A. (2010). An interaction between kynurenine and the aryl hydrocarbon receptor can generate regulatory T cells. J. Immunol. *185*, 3190–3198. https://doi.org/10.4049/jimmunol.0903670.

9. Cady, S.G., and Sono, M. (1991). 1-Methyl-DL-tryptophan, beta-(3-benzofuranyl)-DL-alanine (the oxygen analog of tryptophan), and beta-[3-benzo(b)thienyl]-DL-alanine (the sulfur analog of tryptophan) are competitive inhibitors for indoleamine 2,3-dioxygenase. Arch. Biochem. Biophys. *291*, 326–333. https://doi.org/10.1016/0003-9861(91)90142-6.

10. Prendergast, G.C., Malachowski, W.P., DuHadaway, J.B., and Muller, A.J. (2017). Discovery of IDO1 Inhibitors: From Bench to Bedside. Cancer Res. *77*, 6795–6811. https://doi.org/10.1158/0008-5472.CAN-17-2285.

11. Yue, E.W., Sparks, R., Polam, P., Modi, D., Douty, B., Wayland, B., Glass, B., Takvorian, A., Glenn, J., Zhu, W., et al. (2017). INCB24360 (Epacadostat), a Highly Potent and Selective Indoleamine-2,3-dioxygenase 1 (IDO1) Inhibitor for Immuno-oncology. ACS Med. Chem. Lett. *8*, 486–491. https://doi.org/10.1021/acsmedchemlett.6b00391.

12. Ellington, A.D., and Szostak, J.W. (1990). In vitro selection of RNA molecules that bind specific ligands. Nature *346*, 818–822. https://doi.org/10.1038/346818a0.

13. Tuerk, C., and Gold, L. (1990). Systematic evolution of ligands by exponential enrichment: RNA ligands to bacteriophage T4 DNA polymerase. Science *249*, 505–510. https://doi.org/10.1126/science.2200121.

14. Mayer, G. (2009). The chemical biology of aptamers. Angew Chem. Int. Ed. Engl. *48*, 2672–2689. https://doi.org/10.1002/anie.200804643.

15. Gao, F., Yin, J., Chen, Y., Guo, C., Hu, H., and Su, J. (2022). Recent advances in aptamer-based targeted drug delivery systems for cancer therapy. Front. Bioeng. Biotechnol. *10*, 972933. https://doi.org/10.3389/fbioe.2022.972933.

16. Xu, Y., Jiang, X., Zhou, Y., Ma, M., Wang, M., and Ying, B. (2021). Systematic Evolution of Ligands by Exponential Enrichment Technologies and Aptamer-Based Applications: Recent Progress and Challenges in Precision Medicine of Infectious Diseases. Front. Bioeng. Biotechnol. *9*, 704077. https://doi.org/10.3389/fbioe.2021.704077.

17. Parashar, A. (2016). Aptamers in Therapeutics. J. Clin. Diagn. Res. *10*, BE01-06. https://doi.org/10.7860/JCDR/2016/18712.7922.

18. Zhou, J., and Rossi, J. (2017). Aptamers as targeted therapeutics: current potential and challenges. Nat. Rev. Drug Discov. *16*, 181–202. https://doi.org/10.1038/nrd.2016.199.

19. Carvalho, J., Paiva, A., Cabral Campello, M.P., Paulo, A., Mergny, J.L., Salgado, G.F., Queiroz, J.A., and Cruz, C. (2019). Aptamer-based Targeted Delivery of a G-quadruplex Ligand in Cervical Cancer Cells. Sci. Rep. *9*, 7945. https://doi.org/10.1038/s41598-019-44388-9.

20. Chen, L., Rashid, F., Shah, A., Awan, H.M., Wu, M., Liu, A., Wang, J., Zhu, T., Luo, Z., and Shan, G. (2015). The isolation of an RNA aptamer targeting to p53 protein with single amino acid mutation. Proc. Natl. Acad. Sci. USA *112*, 10002–10007. https://doi.org/10.1073/pnas.1502159112.

21. Huang, B.T., Lai, W.Y., Chang, Y.C., Wang, J.W., Yeh, S.D., Lin, E.P.Y., and Yang, P.C. (2017). A CTLA-4 Antagonizing DNA Aptamer with Antitumor Effect. Mol. Ther. Nucleic Acids *8*, 520–528. https://doi.org/10.1016/j.omtn.2017.08.006.

22. Prodeus, A., Abdul-Wahid, A., Fischer, N.W., Huang, E.H.B., Cydzik, M., and Gariépy, J. (2015). Targeting the PD-1/PD-L1 Immune Evasion Axis With DNA Aptamers as a Novel Therapeutic Strategy for the Treatment of Disseminated Cancers. Mol. Ther. Nucleic Acids *4*, e237. https://doi.org/10.1038/mtna.2015.11.

23. Gao, T., Mao, Z., Li, W., and Pei, R. (2021). Anti-PD-L1 DNA aptamer antagonizes the interaction of PD-1/PD-L1 with antitumor effect. J. Mater. Chem. B *9*, 746–756. https://doi.org/10.1039/d0tb01668c.

24. Soldevilla, M.M., Hervas, S., Villanueva, H., Lozano, T., Rabal, O., Oyarzabal, J., Lasarte, J.J., Bendandi, M., Inoges, S., López-Díaz de Cerio, A., and Pastor, F. (2017). Identification of LAG3 high affinity aptamers by HT-SELEX and Conserved Motif Accumulation (CMA). PLoS One *12*, e0185169. https://doi.org/10.1371/journal.pone.0185169.

25. Thomas, B.J., Porciani, D., and Burke, D.H. (2022). Cancer immunomodulation using bispecific aptamers. Mol. Ther. Nucleic Acids *27*, 894–915. https://doi.org/10.1016/j.omtn.2022.01.008.

26. Patil, S.D., Rhodes, D.G., and Burgess, D.J. (2005). DNA-based therapeutics and DNA delivery systems: a comprehensive review. AAPS J. *7*, E61–E77. https://doi.org/10.1208/aapsj070109.

27. Peyraud, F., Guegan, J.P., Bodet, D., Cousin, S., Bessede, A., and Italiano, A. (2022). Targeting Tryptophan Catabolism in Cancer Immunotherapy Era: Challenges and Perspectives. Front. Immunol. *13*, 807271. https://doi.org/10.3389/fimmu.2022.807271.

28. Liu, M., Li, Z., Yao, W., Zeng, X., Wang, L., Cheng, J., Ma, B., Zhang, R., Min, W., and Wang, H. (2020). IDO inhibitor synergized with radiotherapy to delay tumor growth by reversing T cell exhaustion. Mol. Med. Rep. *21*, 445–453. https://doi.org/10.3892/mmr.2019.10816.

29. Xu, G., Wang, T., Li, Y., Huang, Z., Wang, X., Zheng, J., Yang, S., Fan, Y., and Xiang, R. (2018). A highly potent and selective inhibitor Roxyl-WL targeting IDO1 promotes immune response against melanoma. J. Enzym. Inhib. Med. Chem. 33, 1089–1094. https://doi.org/10.1080/14756366.2018.1471688.

30. Chu, C.L., Lee, Y.P., Pang, C.Y., Lin, H.R., Chen, C.S., and You, R.I. (2020). Tyrosine kinase inhibitors modulate dendritic cell activity via confining c-Kit signaling and tryptophan metabolism. Int. Immunopharm. 82, 106357. https://doi.org/10.1016/j.intimp.2020.106357.

31. Jochems, C., Fantini, M., Fernando, R.I., Kwilas, A.R., Donahue, R.N., Lepone, L.M., Grenga, I., Kim, Y.S., Brechbiel, M.W., Gulley, J.L., et al. (2016). The IDO1 selective inhibitor epacadostat enhances dendritic cell immunogenicity and lytic ability of tumor antigen-specific T cells. Oncotarget 7, 37762–37772. https://doi.org/10.18632/oncotarget.9326.

32. Sica, A., and Massarotti, M. (2017). Myeloid suppressor cells in cancer and autoimmunity. J. Autoimmun. 85, 117–125. https://doi.org/10.1016/j.jaut.2017.07.010.

33. Théate, I., van Baren, N., Pilotte, L., Moulin, P., Larrieu, P., Renauld, J.C., Hervé, C., Gutierrez-Roelens, I., Marbaix, E., Sempoux, C., and Van den Eynde, B.J. (2015). Extensive profiling of the expression of the indoleamine 2,3-dioxygenase 1 protein in normal and tumoral human tissues. Cancer Immunol. Res. 3, 161–172. https://doi.org/10.1158/2326-6066.CIR-14-0137.

34. Guo, Y., Liu, Y., Wu, W., Ling, D., Zhang, Q., Zhao, P., and Hu, X. (2021). Indoleamine 2,3-dioxygenase (Ido) inhibitors and their nanomedicines for cancer immunotherapy. Biomaterials 276, 121018. https://doi.org/10.1016/j.biomaterials.2021.121018.

35. Wan, L.Y., Yuan, W.F., Ai, W.B., Ai, Y.W., Wang, J.J., Chu, L.Y., Zhang, Y.Q., and Wu, J.F. (2019). An exploration of aptamer internalization mechanisms and their applications in drug delivery. Expet Opin. Drug Deliv. 16, 207–218. https://doi.org/10.1080/17425247.2019.1575808.

36. Yang, M.M., Yarragudi, S.B., Jamieson, S.M.F., Tang, M., Wilson, W.R., and Wu, Z. (2022). Calcium Enabled Remote Loading of a Weak Acid Into pH-sensitive Liposomes and Augmented Cytosolic Delivery to Cancer Cells via the Proton Sponge Effect. Pharm. Res. (N. Y.) 39, 1181–1195. https://doi.org/10.1007/s11095-022-03206-0.

37. Voltà-Durán, E., Parladé, E., Serna, N., Villaverde, A., Vazquez, E., and Unzueta, U. (2023). Endosomal escape for cell-targeted proteins. Going out after going in. Biotechnol. Adv. 63, 108103. https://doi.org/10.1016/j.biotechadv.2023.108103.

38. Shcharbin, D., Bryszewska, M., Mignani, S., Shi, X., and Majoral, J.P. (2020). Phosphorus dendrimers as powerful nanoplatforms for drug delivery, as fluorescent probes and for liposome interaction studies: A concise overview. Eur. J. Med. Chem. 208, 112788. https://doi.org/10.1016/j.ejmech.2020.112788.

39. Ruseska, I., Fresacher, K., Petschacher, C., and Zimmer, A. (2021). Use of Protamine in Nanopharmaceuticals—A Review. Nanomaterials 11, 1508.

40. Mellor, A.L., and Munn, D.H. (2004). IDO expression by dendritic cells: tolerance and tryptophan catabolism. Nat. Rev. Immunol. 4, 762–774. https://doi.org/10.1038/nri1457.

41. Sittig, S.P., van Beek, J.J.P., Flórez-Grau, G., Weiden, J., Buschow, S.I., van der Net, M.C., van Slooten, R., Verbeek, M.M., Geurtz, P.B.H., Textor, J., et al. (2021). Human type 1 and type 2 conventional dendritic cells express indoleamine 2,3-dioxygenase 1 with functional effects on T cell priming. Eur. J. Immunol. 51, 1494–1504. https://doi.org/10.1002/eji.202048580.

42. Meireson, A., Devos, M., and Brochez, L. (2020). IDO Expression in Cancer: Different Compartment, Different Functionality? Front. Immunol. 11, 531491. https://doi.org/10.3389/fimmu.2020.531491.

43. Sharma, M.D., Pacholczyk, R., Shi, H., Berrong, Z.J., Zakharia, Y., Greco, A., Chang, C.S.S., Eathiraj, S., Kennedy, E., Cash, T., et al. (2021). Inhibition of the BTK-IDO-mTOR axis promotes differentiation of monocyte-lineage dendritic cells and enhances anti-tumor T cell immunity. Immunity 54, 2354–2371.e8. https://doi.org/10.1016/j.immuni.2021.09.005.

44. Levina, V., Su, Y., and Gorelik, E. (2012). Immunological and nonimmunological effects of indoleamine 2,3-dioxygenase on breast tumor growth and spontaneous metastasis formation. Clin. Dev. Immunol. 2012, 173029. https://doi.org/10.1155/2012/173029.

45. Yamasuge, W., Yamamoto, Y., Fujigaki, H., Hoshi, M., Nakamoto, K., Kunisawa, K., Mouri, A., Nabeshima, T., and Saito, K. (2019). Indoleamine 2,3-dioxygenase 2 depletion suppresses tumor growth in a mouse model of Lewis lung carcinoma. Cancer Sci. 110, 3061–3067. https://doi.org/10.1111/cas.14179.

46. Chen, Y., Xia, R., Huang, Y., Zhao, W., Li, J., Zhang, X., Wang, P., Venkataramanan, R., Fan, J., Xie, W., et al. (2016). An immunostimulatory dual-functional nanocarrier that improves cancer immunochemotherapy. Nat. Commun. 7, 13443. https://doi.org/10.1038/ncomms13443.

47. Qiao, H., Chen, X., Chen, E., Zhang, J., Huang, D., Yang, D., Ding, Y., Qian, H., Feijen, J., and Chen, W. (2019). Folated pH-degradable nanogels for the simultaneous delivery of docetaxel and an IDO1-inhibitor in enhancing cancer chemo-immunotherapy. Biomater. Sci. 7, 2749–2758. https://doi.org/10.1039/c9bm00324j.

48. Ma, P., Ye, H., Guo, H., Ma, X., Yue, L., and Wang, Z. (2022). Aptamer truncation strategy assisted by molecular docking and sensitive detection of T-2 toxin using SYBR Green I as a signal amplifier. Food Chem. 381, 132171. https://doi.org/10.1016/j.foodchem.2022.132171.

49. Teng, I.T., Li, X., Yadikar, H.A., Yang, Z., Li, L., Lyu, Y., Pan, X., Wang, K.K., and Tan, W. (2018). Identification and Characterization of DNA Aptamers Specific for Phosphorylation Epitopes of Tau Protein. J. Am. Chem. Soc. 140, 14314–14323. https://doi.org/10.1021/jacs.8b08645.

50. Li, X., Yang, Y., Zhao, H., Zhu, T., Yang, Z., Xu, H., Fu, Y., Lin, F., Pan, X., Li, L., et al. (2020). Enhanced in Vivo Blood-Brain Barrier Penetration by Circular Tau-Transferrin Receptor Bifunctional Aptamer for Tauopathy Therapy. J. Am. Chem. Soc. 142, 3862–3872. https://doi.org/10.1021/jacs.9b11490.

STAR★METHODS

KEY RESOURCES TABLE

REAGENT or RESOURCE	SOURCE	IDENTIFIER
Antibodies		
Anti-beta actin	Servicebio	Cat# GB15001
Anti-GAPDH	TransGen Biotech	Cat# HC301-01
Anti-Indoleamine 2,3-dioxygenase	Abcam	Cat# ab277522
Anti-Mouse/Rat Foxp3-APC	eBioscience	Cat# 77-5775-40, RRID:AB_469981
APC anti-mouse CD11c	BioLegend	Cat# 117310, RRID:AB_313779
APC anti-mouse F4/80	BioLegend	Cat# 123115, RRID:AB_893493
APC anti-mouse IFN-gamma	BioLegend	Cat 505809, RRID:AB_315403
FITC anti-mouse CD8a	BioLegend	Cat# 100705, RRID:AB_312744
FITC anti-mouse/human CD11b	BioLegend	Cat# 101205, RRID:AB_312788
HA tag	Abcam	Cat# ab18181, RRID:AB_444303
IDO1	CST	Cat# 51851S
PE anti-mouse CD25	Biolegend	Cat 102007, RRID:AB_312856
PE anti-mouse Ly-6C	BioLegend	Cat# 128007, RRID:AB_1186133
PE anti-mouse TNF-alpha	BioLegend	Cat# 506305, RRID:AB_315426
PE/Cyanine7 anti-mouse CD45	BioLegend	Cat# 103113, RRID:AB_312978
PerCP anti-mouse CD4	BioLegend	Cat 100537, RRID:AB_893331
PerCP anti-mouse Ly-6G	Biolegend	Cat# 127653, RRID:AB_2616998
Purified anti-mouse CD3epsilon	BioLegend	Cat# 100302, RRID:AB_312667
Purified anti-mouse CD28	BioLegend	Cat# 102101, RRID:AB_312867
Chemicals, peptides, and recombinant proteins		
Catalase	Sigma-Aldrich	C1345-1G
CCK-8	Bimake	B34304
4-(Dimethylamino)benzaldehyde	Sigma-Aldrich	100-10-7
Ficoll-Hypaque	Dakewe Biotech	7211011
Hoechst	Bioss	D-9105-25mg
Ionomycin	Thermo Scientific	I24222
IPTG	Amresco	0487-1G
L-ascorbic acid	Sigma-Aldrich	V900134-100G
L-kynurenine	Sigma-Aldrich	K8625-25MG
L-tryptophan	Sigma-Aldrich	T8941-100G
Methylene blue	Macklin	M834456-1g
Ni-NTA magnetic beads	Thermo Scientific	88831
PEI	Polysciences	23966-1
Percoll	GE Healthcare Life Sciences	17-0891-09
PMA	Sigma-Aldrich	P1585
Polybrene	Sigma-Aldrich	TR-1003-G
Poly-D-lysine	Beyotime	ST508
Protamine	Sigma-Aldrich	P4020-1G
Protein transport inhibitor cocktail	eBioscience	00-4980-93
Puromycin	MedChemExpress	HY-B1743A
Recombinant mouse IFN-γ	PeproTech	AF-315-05-20UG

Continued

REAGENT or RESOURCE	SOURCE	IDENTIFIER
Recombinant mouse IL-2	PeproTech	212-12-20UG
Recombinant mouse IL-4	PeproTech	214-14-20UG
Recombinant mouse GM-CSF	PeproTech	315-03-20UG
Streptavidin sepharose beads	GE Healthcare Life Sciences	17-5113-01
Trichloroacetic acid	Sigma-Aldrich	T6399
TRIzol	Invitrogen	15596026
Critical commercial assays		
Annexin V-mCherry and SYTOX Green	Beyotime	C1070S
HiScript III All-in-one RT SuperMix	Vazyme	R333-01
TruSeq RNA Sample Prep Kit	Illumina	N/A
Mouse CD3 T Cell Isolation Kit	BioLegend	480023
RNA Nano 6000 Assay Kit	Agilent Technologies	5067-1511
Taq Pro Universal SYBR qPCR Master Mix	Vazyme	Q712-02
Deposited data		
RNA-seq data	This paper	GSE222366
Experimental models: Cell lines		
CT26	ATCC	CRL-2638
HEK293T	ATCC	CRL-11268
Experimental models: Organisms/strains		
Mouse: BALB/c	Charles River	N/A
Mouse: NOD/SCID	Charles River	N/A
Oligonucleotides		
Aptamers, see Table S2	This paper	N/A
DNA library	Teng et al.[49]	N/A
Primer: DNA library forward: CAGCACCGTCAACTGAAT	Teng et al.[49]	N/A
Primer: DNA library reverse: ACATCTCCATCGCATCAC	Teng et al.[49]	N/A
Primer: Actb forward: CGAGGCCCAGAGCAAGAGAG	This paper	N/A
Primer: Actb reverse: CGGTTGGCCTTAGGGTTCAG	This paper	N/A
Primer: Ido1#1 forward: CAAAGCAATCCCCACTGTATCC	This paper	N/A
Primer: Ido1#1 reverse: ACAAAGTCACGCATCCTCTTAAA	This paper	N/A
Primer: Ido1#2 forward: GCCTCCTATTCTGTCTTATGCAG	This paper	N/A
Primer: Ido1#2 reverse: ATACAGTGGGGATTGCTTTGATT	This paper	N/A
Targeting sequence in shIDO1#1: CTGGAGAAAGCCAAGGAAATTT	This paper	N/A
Targeting sequence in shIDO1#2: TTCCACGTTCTCCGCATATAT	This paper	N/A

Continued

REAGENT or RESOURCE	SOURCE	IDENTIFIER
Software and algorithms		
Clustal X	Clustal	Version 2.1
FlowJo	BD Biosciences	Version 10.0.7
GraphPad Prism	GraphPad	Version 6.01
ImageJ	ImageJ	Version 1.50i
NIS-Elements Viewer	Nikon	Version 4.20

RESOURCE AVAILABILITY

Lead contact

Further information and requests for resources should be directed to and will be fulfilled by the lead contact, Yuxin Yin (yinyuxin@bjmu.edu.cn).

Materials availability

All material generated in this study are available from the lead contact upon request.

Data and code availability

RNA-seq data have been deposited at GEO with the accession code GSE222366 and are publicly available as of the date of publication. All data reported in this paper will be shared by the lead contact upon request.

This paper does not report original code.

Any additional information required to reanalyze the data reported in this paper is available from the lead contact upon request.

EXPERIMENTAL MODELS AND STUDY PARTICIPANT DETAILS

Mice

Female BALB/c and NOD/SCID mice were purchased from Charles River Laboratories. 6–8 weeks-old mice were used for the study. All animals were housed and maintained under a specific pathogen-free condition at the Department of Laboratory Animal Science of Peking University Health Science Center with controlled temperature (20–26°C), humidity (40–70%), and 12 h light/dark cycle. The animal experiments were performed following protocols approved by the Ethics Committee of Peking University Health Science Center.

Cell culture

HEK293T cells and the murine colon cancer cell line CT26 from the American Type Culture Collection were cultured in DMEM or RPMI 1640 medium at 37°C and 5% CO_2. All culture media were supplemented with 10% (v/v) fetal bovine serum (FBS), penicillin (100 U/mL), and streptomycin (100 μg/mL). These cell lines do not have mycoplasma contamination.

Lymphocytes isolated from the spleen of an 8 weeks-old female BALB/c mouse were cultured in RPMI 1640 medium supplemented with 10% FBS, 1% L-glutamate, penicillin (100 U/mL), streptomycin (100 μg/mL) at 37°C and 5% CO_2.

Bone marrow cells (BMs) isolated from the tibia and femur of an 8 weeks-old female BALB/c mouse were cultured in RPMI 1640 medium supplemented with 10% FBS, 1% L-glutamate, penicillin (100 U/mL), streptomycin (100 μg/mL) at 37°C and 5% CO_2.

Aptamers

All ssDNA libraries and aptamers were synthesized by Ruibiotech (Beijing, China). The ssDNA library contained 40 random nucleotides flanked by two primer binding sequences referring to a previous study.[49] The sequences of primers for aptamer amplifying were forward, 5'-CAGCACCGTCAACTGAAT-3', and reverse, 5'-ACATCTCCATCGCATCAC-3'.

METHOD DETAILS

Protein expression and purification

The CDS region of Mus musculus *Ido1* mRNA (NM_008324.2) was inserted into the pET28a (+) vector which contains an N-terminal hexahistidine (His6) tag. The vector was transformed into *E. coli* BL21 (DE3), and then induced to express with 1 M IPTG for 4 h at 37°C in LB media. The cell pellet was harvested and re-suspended in TBS buffer with 1 M TCEP and 100 mM PMSF. After sonication and centrifugation, the supernatant was loaded onto Ni- NTA column (Smart-Lifesciences) and successively washed with wash buffer (20 mM Tris, 500 mM NaCl, pH 8.0) and wash buffer containing 20 mM imidazole or 40 mM imidazole. Then the binding protein was eluted with an elution buffer (20 mM Tris, 500 mM NaCl, 60 mM imidazole pH 8.0). Eluted proteins were concentrated by super filters (3 M) and further purified by a molecular sieve (GE Healthcare Life Sciences). The IDO1 protein was quickly frozen in liquid nitrogen and stored at −80°C.

Protein-based SELEX

At the beginning of the screening process, 50 μg recombinant His-tagged mouse IDO1 protein was immobilized to Ni-NTA beads (Smart-Lifesciences). Then the beads were incubated with 5 nmol ssDNA library in binding buffer (10 mM Tris, 150 mM NaCl, 5 mM KCl, 1 mM $MgCl_2$, 1 mM $CaCl_2$, pH 7.5), supplemented with 1 mg/mL BSA and 100 μg/L tRNA, for 1 h at 4°C. In round #4, bare Ni-NTA beads were introduced as negative selection. After washing with washing buffer (10 mM Tris, 150 mM NaCl, 5 mM KCl, 1 mM $MgCl_2$, 1 mM $CaCl_2$, 0.05% (v/v) Tween 20, pH 7.5), sequences bound to the target protein were retrieved in ddH_2O by heating to 95°C for 10 min. The supernatant was collected and subjected to PCR to amplify target binding sequences. Next, 5′ FAM-labeled forward primer and 5′ biotin-labeled reverse primer were used for PCR amplification, and the PCR products were incubated with streptavidin sepharose beads (GE Healthcare Life Sciences) for 30 min at 37°C. NaOH in the concentration of 200 mM was used to separate double-stranded chains of PCR products, and the eluted 5′ FAM-labeled amplicons were neutralized by HCl. Then the ssDNA amplicons pool was put into the next SELEX cycle, and the enrichment of candidates in each round was monitored by flow cytometric analysis. Enriched DNA pools from round #13 were cloned into TA vectors and sequenced.

Aptamer binding assay

To evaluate the binding specificity of the selected candidates, 250 nM 5′ FAM-labeled aptamer candidates were mixed with 1 μL bare beads or 1 μg IDO1-His-coated Ni-NTA magnetic beads (Thermo Scientific) in 100 μL binding buffer for 1 h at 4°C. To evaluate the dissociation constant of IDO-APT, serially diluted 5′ FAM-labeled IDO-APT was incubated with IDO1-His-coated Ni-NTA magnetic beads in 100 μL binding buffer for 1 h at 4°C. After washing with washing buffer, the fluorescence intensity of the beads was measured by flow cytometry (BD Biosciences). The dissociation constant was calculated using the following formula: Y=Bmax × X / (K_D + X), where Y represents the mean fluorescence intensity (MFI), Bmax represents the maximum MFI, and X represents the concentration of aptamers.

In vitro IDO1 enzyme activity assay

Two micrograms of recombinant His-tagged mouse IDO1 protein and 500 nM aptamer were mixed in 50 mM potassium phosphate buffer (pH 7.5) at a volume of 100 μL and incubated at 4°C for 30 min. Subsequently, the mixture was supplemented with 20 mM L-ascorbic acid (Sigma-Aldrich), 100 μg/mL catalase (Sigma-Aldrich), 10 μM methylene blue (Macklin) and 40 μM L-tryptophan (Sigma-Aldrich) and allowed to incubate at 37°C for 30 min. Then, 50 μL 30% (w/v) trichloroacetic acid (Sigma-Aldrich) was added to the reaction solution, and the mixture was incubated at 65°C for 15 min. After centrifugated at 12000 rpm for 10 min, the supernatant was mixed with an equal volume of 2% (w/v) 4-(Dimethylamino) benzaldehyde (Sigma-Aldrich) in acetic acid. The reaction product was read on a plate reader at 490 nm. Kynurenine concentrations were determined from kynurenine standard curves.

For the measurement of IC_{50}, different concentrations of IDO-APT or scrambled APT were used.

For the measurement of the Michaelis-Menten constant (K_m), serially diluted L-tryptophan was used, and the K_m of mouse IDO1 protein was calculated using the following formula: V=V_{max} × [S] / (K_m + [S]), where V is the rate of the reaction, V_{max} is the maximum rate of the reaction, and [S] is the concentration of L-tryptophan. The inhibition constant of aptamers was calculated using the following formula: K_i=IC_{50} / (1 + [S]/ K_m).

Aptamer structure prediction and aptamer-protein docking

The secondary structure of IDO-APT was predicted by the UNAFold Web Server (http://www.unafold.org). The docking prediction of IDO-APT and IDO1 protein was fulfilled on HDOCK SERVER (http://hdock.phys. hust.edu.cn).

Electrophoretic mobility shift assay (EMSA)

EMSA was performed as previously described.[50] A 10 μL mixture containing 100 nM 5′ FAM-labeled IDO-APT and 1 mg/mL mouse IDO1 protein or control protein (BSA, human IDO1) was incubated in a binding buffer for 1 h at 4°C. The sample was loaded onto an 8% native PAGE gel and run in 1 × TBE at 70 V for 10 min and 150 V for 40 min. The gel was visualized by an Amersham Imager 600 (GE Healthcare Life Sciences).

Aptamer-mediated pull-down assay

HEK293T cells were seeded in 60 mm dishes at a count of 1×10^6 and allowed to grow overnight. Subsequently, HEK293T cells were transfected with the vector encoding HA-tagged mouse IDO1 for 48 h. After harvested, HEK293T cells were lysed by ice-cold Co-IP lysis buffer (150 mM NaCl, 1 mM EDTA, 20 mM Tris–HCl pH 8.0, 10% (v/v) glycerol, 0.5% NP40, 100 × PMSF, and 100 × protease inhibitor cocktail). The cell lysates were incubated with 250 nM 5′ biotin-labeled IDO-APT or scrambled aptamer and spun for 2 h at 4°C. Then streptavidin sepharose beads (GE Healthcare Life Sciences) were mixed with cell lysates for 2 h at 4°C to capture the protein-aptamer complex. After washing three times using washing buffer, proteins precipitated by beads were eluted in the loading buffer by heating. Then the sample was loaded on SDS–PAGE subjected to electrophoresis, followed by staining with colloidal silver or immunoblotting with anti-HA (ab18181, 1:5000, Abcam) antibody.

For experiments of the endogenous expression system, CT26 cells were seeded in 60 mm dishes at a count of 1×10^6 and allowed to grow overnight. Recombinant mouse IFN-γ (PeproTech) at 50 ng/mL was used to induce IDO1 expression. The subsequent procedure was the same as above. Finally, the sample was loaded on SDS–PAGE subjected to electrophoresis and immunoblotting with anti-IDO1 (ab277522, 1:1000, Abcam) and anti-GAPDH (HC301-01, 1:5000, TransGen Biotech) antibodies.

Aptamer-protamine mineralized nanoparticle construction

IDO-APT or scrambled aptamer was mixed with protamine (Sigma-Aldrich) in 1 mL DMEM and incubated at room temperature for 30 min to allow the formation of the aptamer-protamine complex. Then 1 M $CaCl_2$ was mixed to precipitate the complex. After centrifugation, the aptamer-protamine complex was resuspended with DMEM. Different ratios of IDO-APT and protamine were tested and electrophoresed on a 2% agarose gel. The morphology of NP-IDO-APT was observed by transmission electron microscopy (TEM) (JEM-1400 PLUS, Leica, German). The size surface zeta-potential of NP-IDO-APT was determined by dynamic light scattering at 25°C.

Serum stability assay

100 nM 5′ FAM-labeled NP-IDO-APT or bare IDO-APT were incubated in RPMI 1640 with 10% (v/v) FBS for 12 h, 24 h, 36 h, 48 h, and 72 h at 37°C. After mixing with the 5 × loading buffer, 10 μL samples were electrophoresed on 2% agarose gel, and the integrity of aptamer was visualized by an Amersham Imager 600.

Aptamer internalization assay

A total of 1×10^5 CT26 cells were seeded in 20 mm glass bottom cell culture dishes (NEST, Wuxi, China) and cultured for 24 h. Cells were added with 500 nM 5′ FAM-labeled NP-IDO-APT or bare IDO-APT and incubated at 37°C for 6 h. Cells were treated with 30 μM Hoechst (Bioss) for 10 min, before being washed thrice with phosphate-buffered saline (PBS). The images were captured by a Nikon TCS A1 microscope.

Immunofluorescence assay

CT26 cells were seeded on the cover glass and exposed to 50 ng/mL recombinant mouse IFN-γ for 24 h. Cells were treated with 200 nM 5′ FAM-labeled NP-IDO-APT or NP-Scr-APT and incubated at 37°C for 12 h before fix. After that, cells were washed twice with PBS, fixed with ice-cold 4% (w/v) formaldehyde in PBS for 15 min, permeabilized with 0.1% (v/v) NP40 in PBS for 15 min, and blocked with 1% (w/v) BSA dissolved in PBS at room temperature for 1 h. Cells were then incubated with anti-IDO1 (51851S, 1:1200, CST)

antibodies at 4°C overnight, followed by incubation with Alexa555-conjugated anti-rabbit antibody (A27039, 1:300, Invitrogen) at room temperature for 1 h after being rinsing by PBS for three times, and stained with 30 μM Hoechst for 10 min, Cells were evaluated with the Nikon A1 microscope for confocal microscopy.

For DCs, the cover glass was incubated with 0.5 mg/mL poly-D-lysine (Beyotime) at room temperature for 1 h to allow the adherence of cells.

Cell-based IDO1 activity assay

CT26 cells or DCs were seeded in a 96-well plate at a cell density of 1×10^4 cells per well and exposed to 50 ng/mL recombinant mouse IFN-γ for 24 h. Subsequently, the old culture medium was replaced with a fresh medium that contained 200 nM NP-IDO-APT, NP-Scr-APT, or NPs. After 24 h, 100 μL supernatants were collected and mixed with 50 μL 30% (w/v) trichloroacetic acid, then the mixture was incubated at 65°C for 15 min. After centrifuged at 12000 rpm for 10 min, the supernatant was mixed with an equal volume of 2% (w/v) 4-(Dimethylamino)benzaldehyde (Sigma-Aldrich) in acetic acid. The reaction product was read on a plate reader at 490 nm. Kynurenine concentrations were determined from kynurenine standard curves.

Expression level measurement

For protein level detection, samples from tumor tissues or culture cells were lysed in ice-cold Co-IP lysis buffer supplemented with 100 × PMSF, and 100 × protease inhibitor cocktail. The protein concentration of lysates was measured by Bradford assay, then adjusted for equal protein content before immunoblot analysis with antibodies described above.

For mRNA level detection, TRIzol reagent (Invitrogen) was used to isolate total RNA from cells or tissues, followed by reverse transcription with HiScript III All-in-one RT SuperMix (Vazyme). Real-time PCR reactions were prepared with Taq Pro Universal SYBR qPCR Master Mix (Vazyme), then analyzed by Applied Biosystems™ 7500. Primer sequences for RT-PCR analysis were as follows: *Actb* forward, 5'- CGAGG CCCAGAGCAAGAGAG-3', and reverse, 5'- CGGTTGGCCTTAGGGTTCAG -3'; *Ido1*#1 forward, 5'- CAAA GCAATCCCCACTGTATCC -3', and reverse, 5'- ACAAAGTCACGCATCCTCTTAAA -3'; *Ido1*#2 forward, 5'- GCCTCCTATTCTGTCTTATGCAG -3', and reverse, 5'- ATACAGTGGGGATTGCTTTGATT -3'.

Cell proliferation assay

CT26 cells were seeded in a 96-well plate at a cell density of 2×10^3 cells per well and allowed to grow overnight. Cells were treated with 100 nM NP-IDO-APT, NP-Scr-APT, or NPs for 24 h, 48 h, and 72 h. Afterwards, 10 μL CCK-8 reagent (Bimake) per well was added and incubated at 37°C for 3 h. The effect of the above treatment on cell proliferation was measured by reading the absorbance at 450 nm.

Apoptosis measurement

CT26 cells were seeded in 12-well plates at a cell density of 1×10^5 cells per well and allowed to grow overnight. Cells were treated with 100 nM NP-IDO-APT, NP-Scr-APT, or NPs at different times. The apoptosis of CT26 cells was determined by a cell apoptosis detection kit with Annexin V-mCherry and SYTOX Green (Beyotime) according to the manufacturer's protocol. Briefly, cells were digested and washed by PBS once, followed by staining with 5 μL Annexin V-mCherry and 1 μL SYTOX Green in 200 μL Binding Buffer for 15 min at room temperature. Stained cells were analyzed by flow cytometry immediately.

In vitro lymphocyte assay

The spleen was harvested from a laboratory BALB/c mouse. After grinding and passing through the 200 meshes strainer, splenocytes were resuspended in RPMI 1640 medium supplemented with 10% FBS, 1% L-glutamate, penicillin (100 U/mL), streptomycin (100 μg/mL), 2 μg/mL anti- mouse CD3 (Cat 100301, Clone 145-2C11, BioLegend), 1 μg/mL anti- mouse CD28 (Cat 102101, Clone 37.51, Biolegend), and 20 ng/mL recombinant mouse IL-2 (PeproTech). A total of 1×10^6 splenocytes per well were seeded into a 12-well plate, treated with 100 nM NP-IDO-APT, NP-Scr-APT, or NPs, and cultured for 6 days. For T cell function measurement, cells were stimulated with 100 ng/mL PMA, 500 ng/mL ionomycin, and protein transport inhibitor cocktail (eBioscience) for 5 h before harvest. Afterwards, cells were incubated with anti-CD45-PE-cy7(Cat 103113, Clone 30-F11, Biolegend), anti-CD8-FITC (Cat 100705, Clone 53-6.7, Biolegend) for surface

staining and incubated with anti-IFN-γ-APC (Cat 505809, Clone XMG1.2, Biolegend) or anti-TNF-α-PE (Cat 506305, Clone MP6-XT22, Biolegend) after fixation and permeabilization. For T_{reg} cells analysis, cells were collected and stained with anti-CD4-PerCP (Cat 100537, Clone RM4-5, Biolegend), anti-CD25-PE (Cat 102007, Clone PC61, Biolegend), and anti-Foxp3-APC (Cat 77-5775-40, Clone FJK-16s, eBioscience). Subsequently, cells were measured by flow cytometry.

RNA sequencing analysis

Purified total RNA was qualified using the RNA Nano 6000 Assay Kit by the Bioanalyzer 2100 system (Agilent Technologies). The transcriptome cDNA libraries were prepared using the Illumina TruSeq RNA Sample Prep Kit and sequenced by the Illumina NovaSeq 6000. After base recognition by CASAVA and quality control using inhouse perl pipeline, clean reads in a fastq format were mapped to the reference genome (mm10) using Hisat2 (v2.0.5). FeatureCounts (v1.5.0-p3) was used to count the number of reads mapped to each gene. Afterwards, the FPKM of each gene was calculated based on the length of the gene and read count mapped to this gene. Gene Ontology (GO) enrichment analysis of differentially expressed genes (DEGs) was implemented by the clusterProfiler R package (v3.8.1). Heatmap of interested genes was performed by the pheatmap R package (v1.0.12).

DCs & T cells coculture assay

BMs from the tibia and femur of 8 weeks BALB/c mice were harvested. After grinding and passing through the 200 meshes strainer, BMs were resuspended in RPMI 1640 medium supplemented with 10% FBS, 1% L-glutamate, penicillin (100 U/mL), streptomycin (100 μg/mL), 40 ng/mL recombinant mouse GM-CSF (PeproTech), and 40 ng/mL recombinant mouse IL-4 (PeproTech) at a density of 5×10^5 cells/mL. BMs were cultured for 6 days to induce BMDCs, and 10 mL fresh medium same as above was supplemented on day 3. After that, the nonadherent cells were collected, and BMDCs were purified by 40% percoll (GE Healthcare Life Sciences). For the identification of DCs, BM-derived DCs were stained with anti-CD45-PE-Cy7 and anti-CD11c-APC.

For the coculture, BMDCs were stimulated with 50 ng/mL recombinant mouse IFN-γ and 1 μg/mL LPS for 24 h. Simultaneously, T cells were isolated from the lymph node of another BALB/c mouse, and CD3$^+$ T cells were purified by the Mouse CD3 T Cell Isolation Kit (BioLegend). Then 1×10^5 BMDCs and 1×10^6 CD3$^+$ T cells mixed in 1 mL RPMI 1640 medium supplemented with 10% FBS, 1% L-glutamate, penicillin (100 U/mL), streptomycin (100 μg/mL) were cocultured in 12-well plates for 6 days with 100 nM NP-IDO-APT, NP-Scr-APT or NPs. At the end of the day, cells were incubated with 100 ng/mL PMA, 500 ng/mL ionomycin, and protein transport inhibitor cocktail for 5 h before harvest. Afterwards, cells were stained with anti-CD45-PEcy7, anti-CD8-FITC, and stained with anti-IFN-γ-APC or anti-TNF-α-PE after fixation and permeabilization.

For the CD3$^+$ T cells culture alone, the condition was the same as above but added with 2 μg/mL anti-mouse CD3, 1 μg/mL anti-mouse CD28, and 20 ng/mL recombinant mouse IL-2.

Short hairpin RNA infection assay

The shRNA targeting *Ido1* was cloned into pLKO.1-puro for gene expression knockdown. Two independent sequences for IDO1 shRNA interference were 5'-CTGGAGAAAGCCAAGGAAATTT-3' and 5'-TTCCACGTTCTCCGCATATAT-3'.

For Lentiviruses production, HEK293T cells were co-transfected with the pLKO.1-puro-sh-IDO1/scramble, the packaging plasmids psPAX2 and pMD2.G. After 48 hours, the culture medium was collected, and passing through 0.45 μM filters. After centrifuging at 20000 rpm at 4°C for 2 h, the lentivirus pellet was resuspended with fresh culture medium and supplemented with polybrene. Then, the medium of CT26 cells was replaced by the lentivirus suspension. In the subsequent culture, 4 μg/ml Puromycin was applied for the selection of stable cell lines.

Mouse syngeneic tumor model

Female BALB/c mice or NOD/SCID mice at 6–8 weeks of age were inoculated subcutaneously with CT26 cells (5×10^5). When the tumor size reached approximately 50 mm^3, mice were randomly separated into three groups: NP-IDO-APT, NP-Scr-APT, or NPs. Then NP-IDO-APT, NP-Scr-APT, or NPs was injected

directly into the tumor three times, respectively at day 6, day 9, and day 12 after seeding. The volume of the tumor was measured using the following formula: $V = L \times S^2 \times 0.5$, where L represents the longest axis and S represents the shortest axis of the tumor. Survival was recorded each day. Tumor-bearing mice were euthanized once the tumor size exceeded 2,000 mm³. To avoid the exhaustion of CD8+ T cells in TILs, the experiment was stopped once significant differences appear in tumor volume between IDO-APT treated group and Scr-APT treated group.

Blood biochemical analysis

Two days after the last treatment, the blood of mice was collected in heparinized tubes and centrifuged at 3000 rpm for 30 min at 4°C. Then supernatants were transferred to new tubes for blood biochemical analysis. ALT and AST were measured to evaluate the liver function, BUN and CREA were detected to assess the renal function.

In vivo IDO1 enzyme activity detection

Levels of Trp and Kyn in the plasma and tumors of CT26 tumor-bearing mice were measured by LC−MS/MS as an indication of IDO enzyme activity. Briefly, 50 µL plasma samples were mixed with an equal volume of water containing 0.1% formic acid (v/v) and vortexed. The mixture was added with 400 µL cold methanol, vortexed and incubated at −20°C for 1 h to precipitate protein. Samples were then centrifuged at 12000 rpm at 4°C for 10 min, and the supernatant was collected for LC−MS/MS measurement. Tumor samples at 50 mg were homogenized in 400 µL water, and the homogenates were mixed with acetonitrile (1:1, v/v). After centrifuging at 12000 rpm at 4°C for 10 min, the supernatants were collected and mixed with equal volumes of methanol to precipitate proteins. The mixture was then centrifuged and supernatants were collected for LC−MS/MS measurement.

Flow cytometric analysis of TILs

The significant differences in tumor volume between IDO-APT treated group and Scr-APT treated group began to appear Mice were euthanized 2 days after the third treatment and the tumor tissue was collected. Tumor tissues were cut into small pieces and digested with collagenase D and DNase I for 30 min at 37°C. After grinding and passing through the 200 meshes strainer, TILs were isolated from the dissociated cells by Ficoll-Hypaque (Dakewe Biotech). For intracellular cytokine analysis, cells were re-stimulated with 100 ng/mL PMA and 500 ng/mL ionomycin in the presence of protein transport inhibitor cocktail for 5 h. After staining with anti-CD45-PE-Cy7 and anti-CD8-FITC, cells were fixed and permeabilized and then stained with anti-TNF-α-PE or anti-IFN-γ-APC. For T$_{reg}$ cells analysis, cells were stained with anti-CD45-PE-Cy7, anti-CD4-FITC, anti-CD25-PE, and anti-Foxp3-APC. For tumor-associated macrophages analysis, cells were stained with anti-CD45-PEcy7, anti-CD11b-FITC (Cat 101205, Clone M1/70, Biolegend), and anti-F4/80-APC (Cat 123115, Clone BM8, Biolegend). For granulocytic or monocytic MDSC analysis, cells were stained with anti-CD45-PEcy7, anti-CD11b-FITC, anti-Ly6C-PE (Cat 128007, Clone HK1.4, Biolegend) or anti-Ly6G-PerCP (Cat 127653, Clone 1A8, Biolegend). The stained cells were then measured by flow cytometry.

QUANTIFICATION AND STATISTICAL ANALYSIS

The results are presented as mean ± SEM using GraphPad software. Statistical significance for comparisons among two groups was analyzed using two-tailed unpaired Student's *t* test or log-rank (Mantel–Cox) test. To compare three or more means, one or two-way ANOVA followed by Tukey's multiple comparisons test was used. The level of significance was set at *$P < 0.05$.